Science of the Total Environment 710 (2020) 136386

Contents lists available at ScienceDirect

Science of the Total Environment

journal homepage: www.elsevier.com/locate/scitotenv

Microbial communities and biogenic Mn-oxides in an on-site biofiltration system for cold Fe-(II)- and Mn(II)-rich groundwater treatment

Sandeepraja Dangeti [a,c], Joyce M. McBeth [b,*], Babak Roshani [c], Jonathan M. Vyskocil [b,1], Brian Rindall [c], Wonjae Chang [a,*]

[a] Department of Civil, Geological, and Environmental Engineering, University of Saskatchewan, Saskatoon, SK, Canada
[b] Department of Geological Sciences, University of Saskatchewan, Saskatoon, SK, Canada
[c] Delco Water Division, Delco Automation, Inc., Saskatoon, SK, Canada

HIGHLIGHTS

- Potential breakthrough for accelerating Mn(II) oxidation kinetics in biofilters
- The low-temperature biofilters selected for bacteria that oxidize Fe(II) and Mn (II)
- Putative bacteria responsible for Mn(II) and/or Fe(II) oxidation were isolated.
- Microbial population enrichment is linked to filter media ripening and chemistry.
- Biogenic birnessite can be a robust indicator for Mn(II)-oxidation in biofilters.

GRAPHICAL ABSTRACT

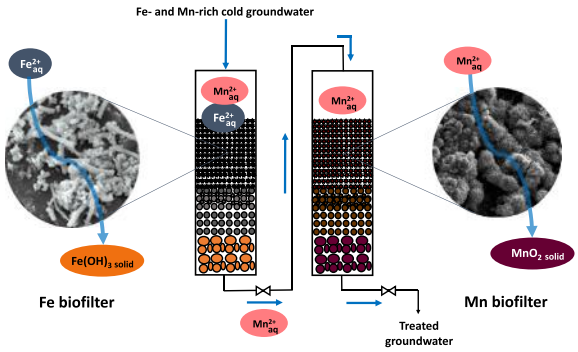

ARTICLE INFO

Article history:
Received 1 November 2019
Received in revised form 26 December 2019
Accepted 26 December 2019
Available online 02 January 2020

Editor: Frederic Coulon

Keywords:
Drinking water treatment
Mn-oxidizing bacteria
Birnessite

ABSTRACT

This study investigated relationships between microbial communities, groundwater chemistry, and geochemical and mineralogical characteristics in field-aged biofilter media from a two-stage, pilot-scale, flow-through biofiltration unit designed to remove Fe(II) and Mn(II) from cold groundwater (8 to 15 °C). High-throughput 16S rRNA gene amplicon sequencing of influent groundwater and biofilter samples (solids, effluents, and backwash water) revealed significant differences in the groundwater, Fe filter, and Mn filter communities. These community differences reflect conditions in each filter that select for populations that biologically oxidize Fe(II) and Mn(II) in the two filters, respectively. Genera identified in both filters included relatives of known Fe(II)-oxidizing bacteria (FeOB), Mn(II)-oxidizing bacteria (MnOB), and ammonia-oxidizing bacteria (AOB). Relatives of AOB and nitrite-oxidizing bacteria were abundant in sequencing reads from both filters. Relatives of FeOB in class *Betaproteobacteria* dominated the Fe filter. Taxa related to Mn-oxidizing organisms were minor members of

Abbreviations: AMOVA, analysis of molecular variance; AOB, ammonia-oxidizing bacteria; BLAST, Basic Local Alignment Search Tool; BWS, initial backwash sludge; CLS, Canadian Light Source; *EDS*, energy dispersive X-ray spectrometry; FeOB, Fe(II)-oxidizing bacteria; Fe filter, iron removal biofilter; Mn filter, manganese removal biofilter; Fe-An, Mn-An, anthracite samples collected from the Fe and Mn filter; Fe-Sa, Mn-Sa, sand samples collected from the Fe and Mn filter; Fe-Ef, effluent samples collected from the bottom of the Fe filter; Fe-BW, backwash material samples from Fe filter; Mn-BW, backwash material samples from Mn filter; EPR, electron paramagnetic resonance; GW, influent groundwater; LBB I, leucoberbelin blue I; LCF, linear combination fitting; MnOB, Mn(II)-oxidizing bacteria; NCBI, National Centre for Biotechnology Information; NOB, nitrite-oxidizing bacteria; ORP, oxidation-reduction potential; OTUs, operational taxonomic units; PCoA, principal coordinate analysis; PCA, principle component analysis; RDP, Ribosomal Database Project; SEM, scanning electron microscopy; SRC, Saskatchewan Research Council; WD, wavelength dispersive; XANES, X-ray absorption near-edge spectroscopy; XRF, X-ray fluorescence.

* Corresponding authors.
E-mail addresses: joyce.mcbeth@usask.ca (J.M. McBeth), wonjae.chang@usask.ca (W. Chang).
[1] present address: Département de Biochimie, Microbiologie et Bio-informatique, Faculté des Sciences et de Génie, Université Laval, Canada.

https://doi.org/10.1016/j.scitotenv.2019.136386
0048-9697/

Biofilter ripening
Low temperatures
Cold climates

the Mn-filter communities; intriguingly, while *Alphaproteobacteria* dominated (40 ± 10% of sequencing reads) the Mn filter community, these *Alphaproteobacteria* did not classify as known MnOB. Isolates from Fe and Mn filter backwash enrichment studies provide insight on the identity of MnOB in this system. Novel putative MnOB isolates included *Azospirillum* sp. CDMB, *Solimonas soli* CDMK, and *Paenibacillus* sp. CDME. The isolate *Hydrogenophaga* strain CDMN can oxidize Mn(II) at 8 °C; this known FeOB is likely capable of Mn(II) oxidation in this system. Synchrotron-based X-ray near-edge spectroscopy (XANES) coupled with electron paramagnetic resonance (EPR) revealed the dominant Mn-oxide that formed was biogenic birnessite. Co-existence of amorphous and crystallized Mn-oxide surface morphologies on the Mn-filter media suggest occurrence of both biological and autocatalytic Mn(II) oxidation in the biofilter. This study provides evidence that biofiltration is a viable approach to remove iron, manganese, and ammonia in cold groundwater systems, and that mineralogical and microbiological approaches can be used to monitor biofiltration system efficacy and function.

1. Introduction

Uncontrolled oxidation of dissolved Mn(II) in groundwater resources used for drinking water production is a common concern (Cerrato et al., 2010). Solid dark brown Mn(III/IV) oxides formed by Mn(II) oxidation cause black discoloration of water and scaling in water distribution facilities, lowering the aesthetic quality of drinking water and damaging water supply infrastructure. High Mn content in water can also elevate the risk of neurobehavioral disorders in children (Bouchard et al., 2011). Dissolved Fe(II) and Mn(II) often coexist in groundwater. Fe(II) oxidation is thermodynamically more favorable than Mn(II) oxidation, and Fe(II) is generally removed from groundwater prior to Mn(II) treatment (Mouchet, 1992).

Microbially-mediated Fe(II) and Mn(II) oxidation promotes removal of excess Fe(II) and Mn(II) from groundwater flowing into fixed-bed biofiltration columns filled with filter media (e.g., anthracite and sand). Mn(II) oxidation is kinetically negligible in the absence of abiotic catalysts and biocatalysts (Katsoyiannis and Zouboulis, 2004). Mn(II)-oxidizing bacteria (MnOB) can thus play a crucial role in the start-up, acclimation, and successful maintenance of Mn(II) removal in biofiltration systems, especially under environmentally-challenging conditions such as low temperature surface water and groundwater regimes in Canada, Alaska, northern Europe, and northern Asia. Biological Mn(II) oxidation is kinetically hindered at low temperatures (Mouchet, 1992), causing long start-up periods and slow Mn(II) removal during biofiltration in these locations (Berbenni et al., 2000; Tekerlekopoulou et al., 2013). Therefore, enriching MnOB that are tolerant to low temperatures is critical for successfully operating biofiltration for groundwater treatment in cold climates.

In addition to biological Mn(II) oxidation, physicochemical Mn (II) oxidation may occur on Mn(III/IV)-oxide surface coatings on filter media. Amorphous biogenic Mn-oxides formed by MnOB exhibit high surface areas that can react with aqueous Mn(II) and act as strong oxidants that subsequently further enhance Mn(II) oxidation (autocatalysis) (Learman et al., 2011; Post, 1999; Sahabi et al., 2009). Bruins et al. (2015b) reported that abiotic Mn-oxides formed by physicochemical oxidation predominated over biogenic Mn-oxide formation on filter media surfaces in a ripened rapid sand filter (RSF). However, a critical difference between biofiltration systems and RSF systems is that RSF systems require oxidizing agent addition, whereas ripening of biofiltration treatment systems is driven by microbial activity. Thus, the characteristics and reactivity of Mn-oxides in a system where biological Mn(II) oxidation is not supplemented with oxidizing agents can differ from those generated in RSF systems. Additionally, the design of biofiltration systems, including the type of media within the biofilters, can have a major influence on the patterns of microbial enrichment in these systems (Breda et al., 2017). Enriching useful MnOB microbial populations (biocatalysts) that are adapted to cold groundwater temperatures could be a crucial step in achieving successful treatment of Mn(II)-rich groundwater under low-temperature regimes and speeding up the treatment process.

Recent studies characterizing the microbiology of groundwater in pilot- and full-scale biofiltration systems using high-throughput sequencing have been conducted at sites with cold (*ca* 7 to 8 °C) groundwater in China (Cheng et al., 2019; Cheng et al., 2017; Zhang et al., 2018). These studies identified enrichment of organisms associated with Fe(II) and Mn(II) oxidation and these genera (*Crenothrix, Ralstonia, Variovorax, Gallionella, Flavobacterium*, and *Microbacterium*) had positive correlations with Mn(II) oxidation in these systems.

This research study addresses a gap in the literature by providing a comprehensive and holistic examination of the synergistic relationships between biological and physicochemical Mn-oxidation in a two-stage, flow-through pilot-scale biofiltration system for the on-site treatment of Fe-(II)- and Mn(II)-rich groundwater under a low temperature regime (8–15 °C) using a broad range of analytical techniques including culture dependent and independent analysis, imaging and elemental analysis, spectroscopic techniques. Our hypotheses were that we would observe the following in a low-temperature biofiltration system: (1) enrichment of both known Fe(II)- and Mn(II)-oxidizing bacteria and other (newly identified) taxa capable of Mn(II)-oxidization, and (2) both biologically-generated and abiotic Mn(III/IV)-oxide precipitates. To address these hypotheses, we investigated microbial communities in a two-stage pilot-scale biofilter operating from 8 to 15 °C installed for the treatment of cold Fe(II)- and Mn(II)-rich groundwater with influent groundwater temperatures ranging from 4 to 8 °C (Fig. 1). The microbiological data were then examined in the context of changes in treated groundwater effluent chemistry (concentrations of Fe(II), Mn(II), NH_3-N, and NO_3^--N) and the characteristics of Mn-oxides associated with biofilter aging (oxidation states, manganese mineralogy, and biogenic/abiotic oxide origins). High-throughput amplicon sequencing (Illumina MiSeq V4 region 16S ribosomal RNA (rRNA) gene) of microorganisms from the biofilters and groundwater, as well as culture-dependent approaches, were used to identify putative MnOB. The Mn oxides that formed on the filter media (solids) were identified and extensively characterized using multiple instrumental analyses, including synchrotron-based X-ray near-edge spectroscopy (XANES), X-ray fluorescence (XRF), scanning electron microscopy (SEM) with energy dispersive X-ray spectrometry (EDS), and electron paramagnetic resonance (EPR).

This comprehensive study reveals the functional enrichment of cold-tolerant microbial communities, including microbial populations acting as FeOB and MnOB in the biofilters. It also shows that biogenic birnessite (Mn-oxide) that formed on the field-aged Mn-biofilter media can be a reliable indicator of successfully-engineered biofiltration that relies on biological and potentially autocatalytic Mn(II) oxidation at low on-site temperatures.

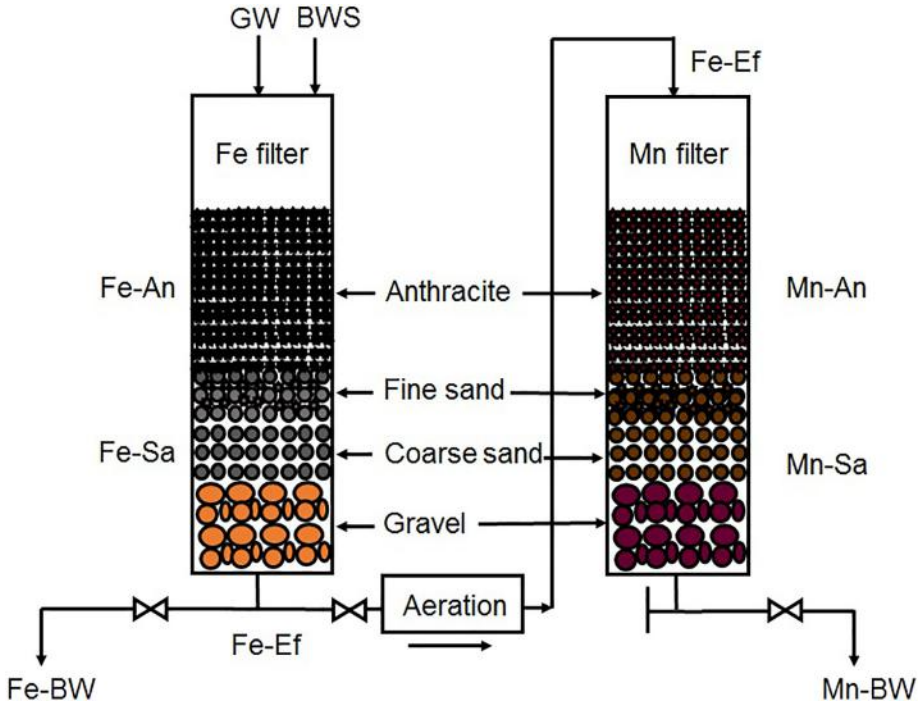

Fig. 1. A schematic representation of the two-stage flow-through pilot-scale biofiltration unit with anthracite, sand, and gravel filter media. The sampling locations and sample types are indicated with arrows in the diagram. Sample abbreviations: GW: influent groundwater; BWS: initial backwash sludge used as an inoculum for the Fe filter; Fe-An: Fe-filter anthracite; Fe-Sa: Fe-filter sand; Fe-BW: Fe-filter backwash; Fe-Ef: Fe-filter effluent; Mn-An: Mn-filter anthracite; Mn-Sa: Mn-filter sand; and Mn-BW: Mn-filter backwash waste.

2. Materials and methods

2.1. Groundwater

The source of the groundwater used in this study was the Floral Formation of the Dalmeny Aquifer. The water was collected from a well at a water treatment plant (WTP) in the Town of Langham (52°21′32.9″N 106°57′02.6″W), 35 km northwest of the City of Saskatoon in Saskatchewan (SK), Canada. Aqueous Fe(II) and Mn(II) are naturally abundant in this groundwater at concentrations of 2.81 ± 0.02 and 0.88 ± 0.01 mg/L, respectively, which exceed the national and provincial aesthetic objective drinking water standards (DWS) for Fe (0.3 mg/L) and Mn (0.02 mg/L) (Health Canada, 2019). The temperature of the incoming groundwater at the Langham WTP is generally stable and varies between 4 and 8 °C, and the temperatures within the biofilter system range from 8 to 15 °C. The oxidation-reduction potential (ORP) of the untreated groundwater varies between −32 and −75 mV, and the pH is 7.90 ± 0.02 (Dangeti et al., 2017).

2.2. Biofiltration performance

The biofiltration unit (Fig. 1), consisted of separate Fe and Mn filter columns (1.55 m high and 0.3 m in diameter). The fixed-bed filters were comprised of four filter-media layers: granular anthracite, fine sand, coarse sand, and gravel. To maintain aerobic conditions, an aerator was installed after the Fe filter to re-oxygenate the water before it entered the Mn filter. The flow velocity for the system was 3.79 m/h, the empty bed contact time (EBCT) was approximately 30 min, and the EBCT-based first-order rate constant for Mn(II) removal after 159 d was 0.21 min^{-1} (Dangeti et al., 2017). The fine and coarse sands and gravel used in the system were standard mesh sizes, and the diameter of the anthracite particles were 1.0–1.1 mm. In order to promote microbial colonization of Fe(II) and Mn(II) oxidizers in the system, we inoculated the Fe filter with backwashed solids from an earlier trial pilot-scale biofiltration system from the same field location.

The pilot-scale biofiltration unit was operated continuously at Langham WTP for 183 days (Dangeti et al., 2017). Briefly, Fe(II) concentrations in the Fe-filter effluent stream rapidly decreased below the DWS of Fe (0.3 mg/L) within five days of operation. The Fe(II) oxidation continued for the duration of the biofiltration experiment. The onset of Mn(II) removal began at around 30 days. A high Mn(II) removal percentage of 97% (bringing the Mn(II) concentrations to below the DWS of 0.02 mg/L) was maintained after 97 days, at which point the mean temperature of the Mn-filter effluent was 12.0 ± 0.6 °C. The ORP of the Mn-filter effluent increased to over +300 mV; this falls in the favorable range for biological Mn(II) oxidation (Mouchet, 1992).

Groundwater, Fe and Mn filter effluents (sampled on Day 106 of operation) were monitored for geochemical changes using inductively coupled plasma optical emission spectroscopy (ICP-OES) and inductively coupled plasma mass spectrometry (ICP-MS) analyses, performed at the Saskatchewan Research Council (SRC). Ammonia-N (NH_3-N) and nitrate-N (NO_3^--N) in the water samples were measured at the SRC using a colorimetric method with an Aquakem 200 Discrete Analyzer (Thermo Scientific). The detection limits for Fe, Mn, ammonia (NH_3-N), and nitrate (NO_3^--N) analyses using ICP-MS/OES or colorimetry were 0.0005 mg/L, 0.0005 mg/L, 0.01 mg/L, and 0.009 mg/L, respectively.

2.3. Sampling and sample nomenclature

A total of 19 samples, including water, backwash sludge and filter media samples, were aseptically collected from the biofiltration unit on Days 110 (for water and backwash sludge samples) and 183 (for inner filter solids) and were shipped in an ice box to the Environmental Engineering Laboratory at the University of Saskatchewan. The shipped samples were immediately processed (by filtration or centrifugation) at the lab. For DNA extractions, each water sample was filtered through a Nalgene® 0.2-μm polyethersulfone (PES) membrane filter. Aliquots of backwash sludge samples (50 mL) were centrifuged (4000*g*, 10 min) and the supernatant was discarded. Samples of the processed samples

and the filter media samples were frozen at either −20 or −85 °C until further sample preparation.

Sample nomenclature used throughout this manuscript corresponds to the sampling locations and sample types (Fig. 1). The influent groundwater and initial backwash sludge inoculant are denoted as GW and BWS, respectively. The BWS was sludge material from an earlier biofiltration system's Fe filter, and it was used as an inoculant for start-up of the Fe filter in the system reported in this manuscript. The anthracite and sand samples collected from the Fe and Mn filters are designated as Fe-An and Mn-An, and Fe-Sa and Mn-Sa, respectively. Fe-Ef refers to groundwater effluent samples collected from the bottom of the Fe filter (this effluent flowed into an aerator and then into the Mn filter). Backwash water samples from Fe and Mn filters are denoted as Fe-BW and Mn-BW, respectively. The 19 samples, including GW samples in triplicate and all other samples (BWS, Fe-Ef, Fe-An Mn-An, Fe-Sa, Mn-Sa, Fe-BW and Mn-BW) in duplicate, were analysed using high-throughput sequencing analyses. Mn-oxides in a subset of these samples were also characterized using chemical and mineralogical methods.

2.4. DNA extraction and high-throughput amplicon sequencing

Genomic DNA was extracted from the 19 samples using PowerWater® DNA Isolation Kits (MoBio Laboratories). For solid samples, 0.5 g of material was extracted; for each water sample, 19 L of water was filtered, and the filter was extracted. The DNA concentrations of the samples were measured using the Qubit® dsDNA High Sensitivity Assay kit (Thermo Scientific Canada); values ranged between 0.1 and 20.8 ng/μL. DNA purity (A260/A280: 1.7 ± 0.3 for the 19 samples) was determined using a NanoDrop 1000 (Thermo Scientific Canada).

The extracted DNA samples were sequencing on an Illumina MiSeq sequencing platform (RTL Genomics, Lubbock, Texas) over the V4-region of the 16S rRNA bacterial and archaeal genes using the Earth Microbiome Project universal primers (515F 5′-GTGCCAGCMGCCGCGGTAA-3′ and 806R 5′-GGACTACHVGGGTWTCTAAT-3′) (Caporaso et al., 2011). The paired-end reads were processed using the mothur software package, version v.1.32 (Schloss et al., 2009). The mothur Illumina MiSeq standard operating procedure (SOP) was used to align, filter, trim, remove chimeras, and classify and assign taxonomy to the reads. Briefly, read pairs were combined into contigs and screened to remove short reads with degenerate bases or reads with homopolymers of 8 bases or greater. The screened sequences were aligned using the SILVA rRNA database for bacterial and archaeal small-subunit rRNA reference alignments (v.119), and pre-clustered with the single-linkage algorithm. Chimeras were identified using UCHIME (the most abundant sequence reads were used as references) and removed (Edgar et al., 2011; Schloss et al., 2011). The sequences were then classified using the Bayesian algorithm of the Ribosomal Database Project (RDP) classifier with a minimum bootstrap confidence cut-off of 80% (Wang et al., 2007). The lowest number of sequence reads obtained from the 19 samples was 8209; thus, the sequence reads were subsampled to 8000 per sample prior to alpha and beta community analyses. The subsampled reads were clustered into operational taxonomic units (OTUs) at 0.03 distance level (97% sequence similarity) using the average neighbor algorithm in mothur.

Rarefaction curves, Good's coverage values, and the Shannon diversity index (H′) were calculated using the mothur community diversity calculators (Schloss and Handelsman, 2005). The Shannon diversity index was used to calculate the Evenness (J′) based on Pielou's evenness index ($J' = H'/\ln(S)$; S=OTUs) and effective number of species ($e^{H'}$) ($e^{H'} = \exp(H')$) (Blackwood et al., 2007). To examine beta diversity, OTU-based distance matrices were created using Yue & Clayton theta values (Yue and Clayton, 2005) via the mothur "dist.shared" command. Principal coordinate analysis (PCoA) plots for the sequence reads were constructed to visualize sample clustering, and analysis of molecular variance (AMOVA) was used to determine significant differences between the microbial compositions of the samples. The corr.axes command (using the Spearman method) was used to calculate correlation vectors to identify how OTUs shifted the position of samples along the axes in the PCoA diagram.

2.5. MnOB isolation

MnOB were isolated from 10^{-2} and 10^{-3} dilutions (in phosphate buffered saline) of the GW, Fe-Ef, Fe-BW, and Mn-BW samples on J agar medium (Nealson, 2006; Tebo et al., 2007). Replicate cultures were incubated in the dark at 8 and 17 °C. Pure cultures were isolated by iterative plate streaking (at least five times) at room temperature. Plates were incubated for 4–8 weeks in each iteration, then transferred to flasks containing J medium and incubated at 22 °C (Tebo et al., 2007). Mn(II)-oxidation activity was confirmed in these isolates by adding 0.04% leucoberbelin blue I (LBB I) to the brown precipitates that formed in the flasks (Cerrato et al., 2010). Genomic DNA from the cultured putative MnOB isolates was extracted using the PowerWater® DNA Isolation Kit as per manufacturer's instructions (MoBio Laboratories). The extracted DNA was used as a template for partial 16S rRNA gene amplification by polymerase chain reaction (PCR) on a Veriti™ Thermal Cycler (Applied Biosystems) using the universal primers 27F (5′-AGAGTTTGATCMTGGCTCAG-3′) and 1492R (5′-GGWTACCTTGTTACGACTT-3′) (obtained from Sigma-Aldrich). Each 50 μL of PCR reaction mixture contained 1 μL of template DNA (or PCR water for the negative control), 27.5 μL of Econotaq Plus 2× mix (Lucigen), primers (10 μM), and PCR-grade water. The amplification protocol was as follows: an initial denaturation of 94 °C for 2 min; 30 amplification cycles (30 s at 94 °C, 30 s at 54 °C, 90 s at 72 °C); and a final extension of 72 °C for 10 min. PCR amplifications for each isolate were conducted in triplicate. The presence and the size of amplified 16S rRNA gene amplicons in the PCR products were confirmed using gel electrophoresis (Lonza- FlashGel™ DNA system, 1.2% agarose, 13 well), replicates were pooled, and the samples were sequenced with 27F and 1492R sequencing primers at the Genome Quebec Innovation Centre, McGill University. The forward and reverse 16S rRNA gene sequences were assembled into contigs and were manually curated using Sequencher software (Gene Codes Corporation). The curated 16S rRNA gene contig sequences were compared using the Basic Local Alignment Search Tool (BLAST) and Genbank 16S rRNA gene sequences (Bacteria and Archaea) database on the National Centre for Biotechnology Information (NCBI) website (https://www.ncbi.nlm.nih.gov/genbank/). RDP version 11.4 was used to determine the species similarity and to assign the taxonomic affiliation (Cole et al., 2014) (https://rdp.cme.msu.edu/seqmatch/seqmatch_intro.jsp).

2.6. XANES analyses

We performed XANES analysis of our samples to obtain chemical information on the manganese phases. We anticipated that the manganese phases in these samples would include amorphous phases, which cannot be identified using powder X-ray diffraction (PXRD) analysis; XANES can provide chemical information on both amorphous and crystalline phases. XANES analyses were performed on the IDEAS beamline (08B2-1) at the Canadian Light Source (CLS) synchrotron in Saskatoon, SK. The beamline was equipped with a Ge(220) crystal monochromator and XANES spectra were collected in fluorescence mode employing a single element Ketek AXAS-M (M5T1T0-H80-ML5BEV) silicon drift detector. Scans were collected over the Mn K-edge (6539 eV) region from −50 eV to −20 eV (step size 1 eV, 3 s dwell time), and −20 eV to +100 eV (step size 0.3 eV, dwell time 3 s). Two to eight scans were collected for each sample to improve the signal-to-noise ratio. A Mn (0) metal mesh was used to calibrate the monochromator, based on the first derivative of the K-edge for Mn(0). Commercial chemical standards were used to obtain edge positions for several Mn-oxidation states: Mn(II)SO_4 (Sigma-Aldrich, 99% pure), Mn(III) oxide (Sigma-Aldrich, 99% pure), Mn(IV) oxide (Sigma-Aldrich, 99% pure), and KMn

(VII)O_4 (Sigma-Aldrich, 99% pure). The filter samples (Fe-BW, Fe-An, Fe-Sa, Mn-BW, Mn-An, and Mn-Sa) were air-dried in a desiccator, ground with a mortar and pestle, and diluted with boron nitride. The samples were loaded into sample holders and sealed in the holders with Kapton tape. Manganite, birnessite, pyrolusite, and bixbyite were used as mineral standards; J. Dynes (CLS) supplied the birnessite sample and the remainder of the samples were acquired from the University of Saskatchewan Geological Sciences mineral collection.

The Athena program (https://bruceravel.github.io/demeter/) (Ravel and Newville, 2005) was employed for XANES data analysis. The Mn K-edge absorption edge position for each sample (Fe-BW, Fe-An, Fe-Sa, Mn-BW, Mn-An, and Mn-Sa) was obtained based on the position of the first derivative of the K-edge. A linear regression model was applied to these values to determine the oxidation states (valences) of the Mn absorption edges (eV) in the XANES spectra of the standards and filter samples (Nam et al., 2007). Principal component analysis (PCA) and linear combination fitting (LCF) were conducted using Athena to determine the proportions of each Mn phase in the Mn-filter samples (Mn-An, Mn-Sa, and Mn-BW). The R-factor and reduced chi-squared (χ^2) values were used to verify the goodness of fit and to check for reliability and consistency of replicate scans.

2.7. XRF and SEM-EDS

The anthracite filter media samples (Fe-An and Mn-An) collected from the Fe and Mn filters on Day 183 (the end of the biofiltration experiment) were sent to the Saskatchewan Research Council (SRC) in Saskatoon for XRF and SEM-EDS analyses. Briefly, the elemental composition of the anthracite surface coatings was determined by Wavelength Dispersive (WD) XRF (S8-Tiger Bruker) with XS-55, PET, and Li200 analyzer crystals. Samples were prepared using the loose powder method and loaded onto Teflon containers with Mylar windows. Geochemical standards GSP2 and DC73301 were used to calibrate the instrument.

SEM-EDS was employed to characterize the morphology and elemental composition of the anthracite samples. The carbon-coated anthracite was analysed using a QEMSCAN 650F equipped with two energy dispersive X-ray detectors (Bruker 5030). EDS measurements were taken at locations where crystal morphologies were consistent with the presence of Mn-oxides. The samples were observed in secondary electron mode at an acceleration potential of 10 to 15 keV and a working distance of 10 mm.

2.8. EPR analyses

To identify the origins (biogenic or abiotic) of Mn-oxides from air-dried, ground Mn-filter samples (Mn-BW, Mn-An, and Mn-Sa), EPR analysis was performed at 295 K, using an X-band Bruker EMX EPR spectrometer (9.8 GHz) in the Saskatchewan Structural Sciences Centre (SSSC) at the University of Saskatchewan. Chemically-synthesized birnessite mineral (provided by J. Dynes, CLS) was used as the reference standard (Hardie et al., 2007). The EPR spectral data was processed using the Xenon software package (version 1.1b60, Bruker Organization). The line width (ΔH in gauss; distance between the highest and lowest points of the first-order signal wave) in the EPR spectra was used to clarify the results as either biogenic or abiotic Mn-oxides. Kim et al. (2011) report that biogenic, biomineral, and abiotic origins of Mn-oxides exhibit ΔH values of <600, 600 to 1200, and >1200, respectively.

2.9. Accession numbers

The raw sequence reads of the 19 high-throughput sequencing sample datasets were deposited into the European Nucleotide Archive (ENA) database of the *European Molecular Biology Laboratory* (http://www.ebi.ac.uk/ena) under project number PRJEB15260 (accession numbers ERS1310608 to ERS1310626; http://www.ebi.ac.uk/ena/data/view/PRJEB15260). The curated isolate 16S rRNA gene sequences were also deposited with the ENA (accession numbers LT628526 to LT628536).

3. Results

3.1. Microbial diversity indices

Nineteen samples including samples from the influent groundwater and biofiltration unit were analysed using high-throughput amplicon sequencing of the 16S rRNA gene (refer to Fig. 1 and the Materials and Methods section for sample nomenclature). The samples analysed also included biological replicates for each sample. With an average length of 275 bp, a total of 288,116 reads passed all quality filtering in mothur (Table 1). The number of sequence reads per sample ranged from 8209 to 28,265. Rarefaction curves for the subsampled quality filtered read data are presented in Fig. S1.

Alpha community analyses of the high-throughput sequencing data (Table 1) showed groundwater community samples had greater richness and diversity than the biofilter community samples. Good's coverage estimator for all samples ranged from 0.95 to 0.99 (mean 0.98, SD 0.01). The richness (operational taxonomic units, OTUs) of the groundwater (GW) ranged from 467 to 966 (mean 726, SD 250), which was generally higher than the filter samples (Fe-An, Fe-Sa, Fe-BW, Mn-An, Mn-Sa, and Mn-BW) which had richness values of 182 to 486 (mean 329, SD 85). The microbial communities in the continuously flowing effluent stream from the Fe filter (Fe-Ef) had higher richness values (640 and 714, n = 2) than the filter samples. The biofilter microbial communities exhibited lower diversity indices (i.e., richness, Shannon index, effective diversity number, and evenness) than the GW communities (Table 1). The mean effective diversity number ($e^{H'}$) for the GW communities was 191 ± 30, whereas the Fe- and Mn- filter inner solid sample communities exhibited lower mean $e^{H'}$ values of 30 ± 4 (Fe-An 1, Fe-An 2, Fe-Sa 1, and Fe-Sa 2) and 50 ± 10 (Mn-An 1, Mn-An 2, Mn-Sa 1, and Mn-Sa 2), respectively. The evenness (J′) of the GW communities was 0.8 ± 0.03, which was closer to 1.0 than the Fe- and Mn- filter inner solid samples (0.58 ± 0.03 and 0.69 ± 0.03, respectively).

3.2. PCoA, AMOVA, and taxonomic analyses

Principal coordinate analysis (PCoA) (Figs. 2, S2) was used to compare the influent groundwater and biofilter communities based on Yue & Clayton's measure of community dissimilarity. The GW, Fe-filter, and Mn-filter communities clustered in distinct regions of the PCoA plot. The GW community plotted closer to the Fe-Ef community (orange squares in Figs. 2 and S2) than to the biofilter communities (remainder of the symbols in shaded areas of Fig. 2). Correlation vectors for selected abundant taxa of interest (Fig. 2, dashed arrows) illustrate that Fe(II)-oxidizing bacteria reads (*Gallionella* and *Sideroxydans)* are correlated with the position of the Fe biofilter communities in the PCoA diagram, but not the Mn biofilter communities. Numerous taxa associated with nitrogen cycling were strongly correlated with the Mn biofilter communities, including Bacteria that are nitrate reducers (*Opitutus*), nitrite oxidizers (*Nitrospira*), nitrogen fixers (*Rhizobiales*), and aerobic ammonia oxidizers (*Nitrosomonas*) (Chin et al., 2001; Kuypers et al., 2018). High read proportions of *Hydrogenophaga*, a putative MnOB (Marcus et al., 2017; Sjöberg et al., 2018), and reads classifying to order *Holophagae* (which includes the genus *Geothrix*, an Fe(II)-reducing bacterium) were also correlated with the position of the Mn biofilter samples in the PCoA diagram.

Statistical analyses of community relationships using AMOVA indicated that the GW community was statistically different from the Fe-filter communities, including the inner filter and effluent samples (Fe-An, Fe-Sa, Fe-BW, BWS, and Fe-Ef) ($p < 0.0001$; Table S1). The Mn-filter communities (Mn-An, Mn-Sa, and Mn-BW) were also significantly different from the GW community ($p = 0.009$), the inner Fe-filter

Table 1
Community coverage, richness, diversity, and evenness measured for high-throughput sequencing data from groundwater, initial backwash sludge, Fe-filter, and Mn-filter communities.

Filter	Sample	Number of sequences	Good's coverage[a,b]	Richness[a,b]	Diversity estimate[a,b]		Evenness[a,b]	Accession number
				OTUs[#] (S)	H′	$e^{H'c}$	J′[c]	(Project number: PRJEB15260)
Groundwater	GW 1	11375	0.99	467	5.1	157	0.82	ERS1310618
	GW 2	19068	0.97	745	5.4	215	0.81	ERS1310619
	GW 3	12567	0.95	966	5.3	200	0.77	ERS1310620
Initial backwash sludge[*]	BWS 1	8209	0.98	360	2.6	13	0.43	ERS1310614
	BWS 2	25643	0.98	403	2.8	17	0.47	ERS1310615
Fe filter	Fe-BW 1	9161	0.98	301	1.9	6	0.33	ERS1310610
	Fe-BW 2	10492	0.99	283	2.2	9	0.38	ERS1310611
	Fe-An 1	8669	0.98	354	3.2	25	0.55	ERS1310608
	Fe-An 2	21085	0.98	392	3.4	29	0.57	ERS1310609
	Fe-Sa 1	20527	0.99	328	3.5	34	0.61	ERS1310616
	Fe-Sa 2	9507	0.98	350	3.5	32	0.59	ERS1310617
	Fe-Ef 1	11229	0.96	640	3.3	27	0.51	ERS1310612
	Fe-Ef 2	9540	0.96	714	3.7	40	0.56	ERS1310613
Mn filter	Mn-BW 1	9389	0.97	445	4.2	65	0.68	ERS1310623
	Mn-BW 2	22228	0.97	486	4.3	71	0.69	ERS1310624
	Mn-An 1	28265	0.99	223	3.6	38	0.67	ERS1310621
	Mn-An 2	22662	0.99	182	3.4	31	0.66	ERS1310622
	Mn-Sa 1	14824	0.99	307	4	57	0.71	ERS1310625
	Mn-Sa 2	13676	0.99	295	4.1	60	0.72	ERS1310626

Abbreviations: OTU, operational taxonomic unit; H′, Shannon diversity index; $e^{H'}$, effective number of species; J′, Pielou's evenness.
The GW, Fe-BW, Fe-Ef, and Mn-BW samples were collected after 110 days of operation; Fe-An, Fe-Sa, Mn-An, and Mn-Sa samples were collected after 183 days of operation; BWS samples were collected from trial experiment at the Langham water treatment plant.
[*] BWS was used as inoculum to Fe filter at start of experiment.
[#] OTUs calculated at 97% sequence similarity.
[a] All samples are subsampled to 8000 sequences.
[b] Sequences are clustered using the average-neighbor method.
[c] Diversity estimates and evenness were calculated based on Shannon index.

communities ($p < 0.0001$), and the Fe-filter effluent community ($p = 0.008$) (Table S1) composition.

For the 19 samples, 99.9% of the total subsampled sequence reads could be taxonomically assigned using the RDP database at a minimum bootstrap confidence cut-off of 80%. At the genus level, 487 taxa (473 Bacteria and 14 Archaea) were identified from the sequence reads. The GW and biofilter communities (both the Fe and Mn biofilters) were dominated by Bacteria (92 ± 2 and 99 ± 2%, respectively). Archaea in the GW communities represented 8 ± 2% of the total sequence reads.

At the phylum level, *Proteobacteria* dominated all samples, representing (40 ± 4, 79 ± 7, and 67 ± 9% of the sequence reads in

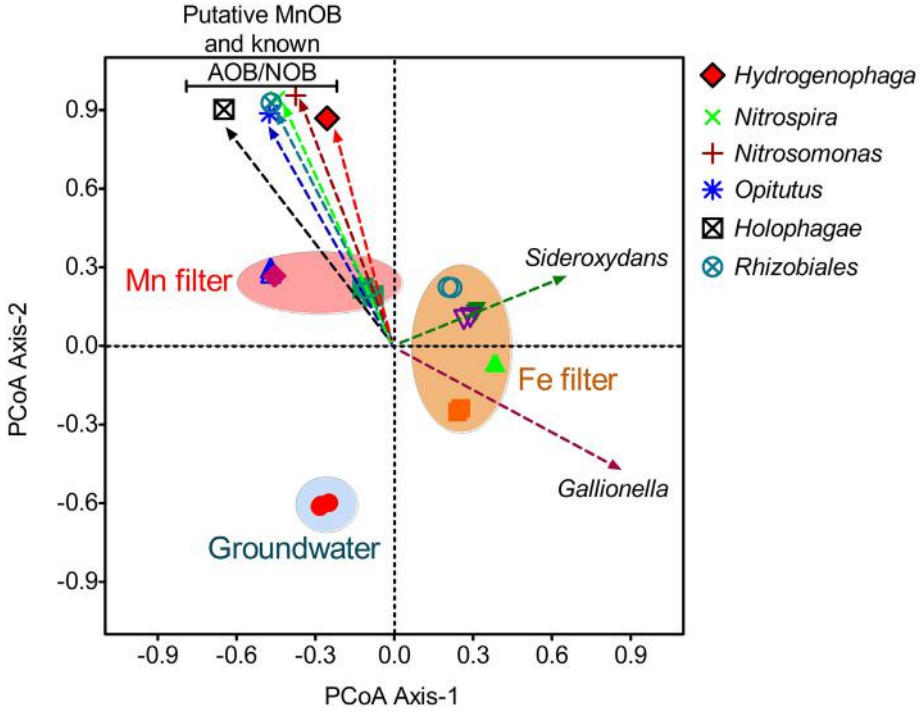

Fig. 2. The principal coordinate analysis (PCoA) plots for sequence reads from the GW, Fe- and Mn-filter-associated samples based on operational taxonomic unit (OTU) distance matrices created using Yue & Clayton theta values. The OTU clusters were defined using a 97% similarity threshold. Shaded circles indicate groupings of sample types (refer to Fig. S2 for version including individual sample labels). Dashed arrows represent correlation vectors for selected taxa of interest.

the GW, Fe-filter, and Mn-filter communities, respectively (Fig. 3A). Bacteria belonging to the *Nitrospirae* and *Verrucomicrobia* phyla were enriched in the Mn filter-associated communities (12 ± 7 and 5 ± 1%, respectively) in comparison with the groundwater communities. The proportions of the *Proteobacteria* classes (Fig. 3B) varies across the GW, Fe-filter and Mn-filter communities considerably. The GW community mainly consisted of *Betaproteobacteria* (39 ± 6%), *Gammaproteobacteria* (31 ± 8%), and *Deltaproteobacteria* (17 ± 4%). In contrast, *Betaproteobacteria* dominated the *Proteobacteria* in the Fe-filter communities (BWS, Fe-An, Fe-Sa; 87 ± 4%). The abundance of *Alphaproteobacteria* in the Mn filter samples (Mn-An, Mn-Sa, and Mn-BW) was higher than in the GW and Fe-filters (40 ± 10%).

3.3. Chemical data and genus-level patterns in sequencing read abundance

Concentrations of Fe, Mn, and NH_3-N in the groundwater and in the effluent from the two filters at Day 110 of the experiment are plotted in Fig. 4 against the abundance of common genera in the biofiltration system. The concentrations of Fe, Mn, and NH_3-N in the influent groundwater were 2.8, 0.9, and 0.53 mg/L, respectively. The Fe concentration was 0.018 mg/L (below the drinking water standard; DWS) in the Fe filter effluent, while Mn and NH_3-N concentrations were unchanged. In the Mn filter effluent, the concentration of Mn was 0.0036 mg/L (also below the DWS), the NH_3-N concentration was 0.13 mg/L, and the NO_3^--N concentration increased to 0.49 mg/L (from <0.009 mg/L in GW). The XRF analyses of the Fe and Mn filters confirmed Fe and Mn precipitates were present on the filter media (Table S2). In the Fe-An sample, the XRF analyses showed a larger quantity of Fe precipitates (4.3%, w/w) than Mn precipitates (0.03%, w/w), whereas Mn precipitates (2.9%, w/w) exceeded Fe precipitates (0.03%, w/w) in the Mn-An samples.

A heat map (Fig. 4) of the top 70 genera from the four microbial habitats in the biofiltration system (GW, BWS, Fe filter, and Mn filter) was constructed based on the percentage of sequence reads in each sample, including unclassified genera. To determine these top 70 genera, we took the top 30 genera from each filter component and inoculum source (Fe filter, Mn filter, groundwater, backwash sludge inoculum; 120 genera total), sorted by abundance for each component/source, merged

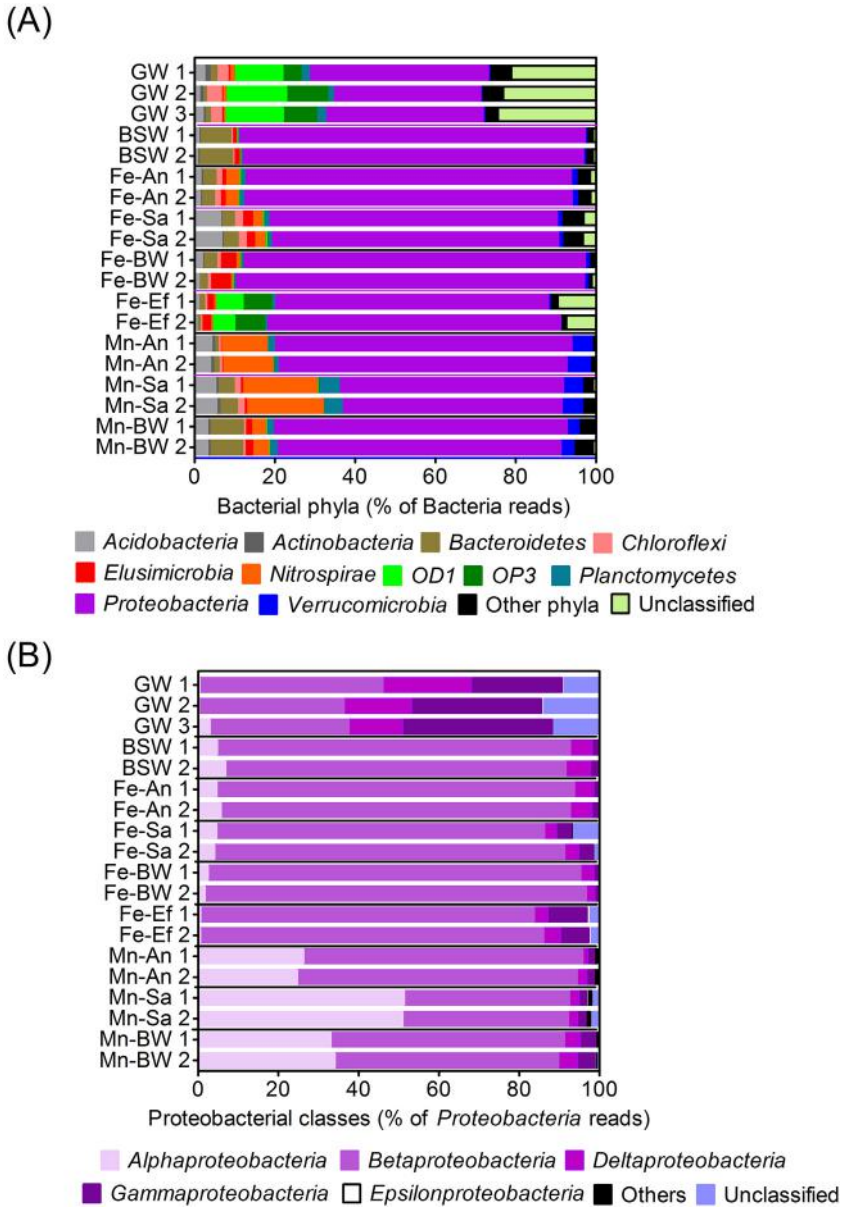

Fig. 3. The community compositions in the GW and Fe and Mn filters at (A) the phylum level and (B) Proteobacterial class level. Results show percent of total sequence reads for each sample type.

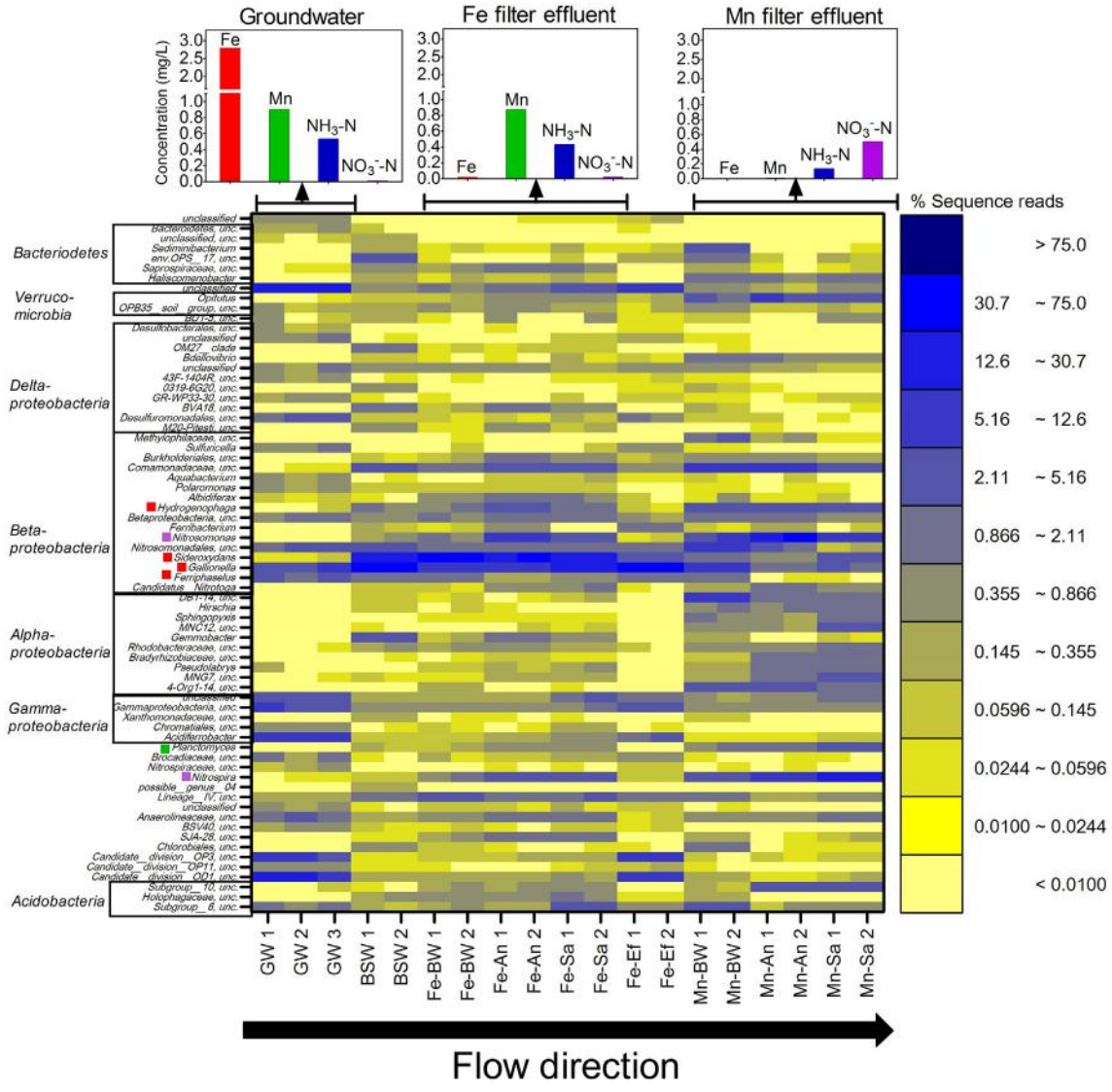

Fig. 4. A heat map for the 70 most abundant bacterial genera (including unclassified genera) in the sequence reads from the 19 high-throughput amplicon sequencing analysis samples (GW and Fe- and Mn-filter samples). In the heat map, red, green, and purple boxes indicate relatives of known FeOB, MnOB, and AOB or NOB, respectively (unc.: unclassified genus). Note that the heat map is on a log scale. Water chemistry data graphs show ICP-MS results for groundwater and effluent water samples from each filter. (For interpretation of the references to color in this figure legend, the reader is referred to the web version of this article.)

duplicate genera across the components/sources, and took the top 70 most abundant genera from the resulting list. The samples are place in the heat map according to their phylogeny (y-axis) and position in the biofiltration system (x-axis; i.e., from influent GW to effluent stream along the direction of flow through the biofiltration unit). The heat map illustrates differences in the read proportions of the representative genera from the influent groundwater to the Fe and Mn filters (e.g., change from darker blue pixels representing abundant genera, to yellow pixels representing lower abundance). Shared genera that were present in high abundance in both the Fe and Mn filter samples (e.g., patches of grey to blue pixels extending from the centre to the right side of the figure) included genera that are likely core microbiome members (e.g., nitrogen cyclers), and genera that include microbes capable of Fe and/or Mn oxidation (the dominant biogeochemical processes in the filters).

3.4. FeOB, MnOB, AOB, and NOB

The top genera by sequence read abundance in the biofiltration system (Fig. 4) included known relatives of FeOB, MnOB, ammonia-oxidizing bacteria (AOB), and nitrite-oxidizing bacteria (NOB). A high proportion of reads in the Fe-filter communities classified as relatives of the known FeOB *Gallionella* (Hallbeck et al., 1993) and *Sideroxydans* (Liu et al., 2012) (20 ± 20% and 30 ± 20%, respectively). Other well-known FeOB relatives in the *Betaproteobacteria* (*Ferriphaselus, and Hydrogenophaga*) were also in the top genera identified in the Fe filter. Interestingly, the known FeOB genera *Gallionella*, *Sideroxydans*, *Hydrogenophaga* (Chan, 2015), and *Ferriphaselus* (Kato et al., 2014), appeared in the top genera in both the Fe- and Mn-filter communities.

Relatives of genera that include organisms capable of Mn(II) oxidation including *Planctomyces* (Schmidt et al., 1981) and *Hydrogenophaga* (Marcus et al., 2017; Sjöberg et al., 2018) are present in the core taxa for the Fe and Mn filters. Relatives of other known MnOB belonging to the genera *Pseudomonas*, *Hyphomicrobium, Albidiferax, Athrobacter*, *Acinetobacter*, *Zoogloea*, *Ralstonia,* and *Pedomicrobium* (Akob et al., 2014; Beukes and Schmidt, 2012; Tebo et al., 2005) were also detected in both the Fe- and Mn-filter communities; however, their read abundances were low in both filters (<1% of sequence reads each), and were thus not included in the heat map. Relatives of known AOB in genus *Nitrosomonas* (Arp et al., 2002) were identified in both biofilters, with higher proportions in the Mn filter (20 ± 10%) than in the Fe filter (6 ± 3%). Similarly, relatives of the known NOB *Nitrospira* (Lücker et al.,

2010) were present in higher proportions in the Mn filter (15 ± 4%) than in the Fe filter (2.8 ± 0.4%).

Many unclassified genera were also enriched in the microbial communities of the Fe and Mn filters in comparison with the GW samples (Fig. 4). From the survey of the 70 genera within the heat map, only 24 genera had been reported in the literature at the time of this study. The remaining 46 genera were unclassified. These unclassified genera comprised 66 ± 3%, 21–23% (n = 2), 25 ± 8%, and 31 ± 9% of the sequence reads in the GW, BWS, Fe filter, and Mn filter, respectively. Given the increased abundance of *Alphaproteobacteria* reads in the Mn filter (Fig. 3) it is interesting that the *Alphaproteobacteria* identified in the Mn filter were mostly unclassified at the genus level (Fig. 4) and did not include genera previously known to be capable of Mn(II) oxidation.

3.5. Putative new MnOB isolates

A total of 11 isolates were cultured from the Fe and Mn filter samples (Table 2), and 10 of the isolates tested positive in the LBB I assay for Mn (III/IV) oxide formation. Of these, *Azospirillum* sp. CDMB, *Solimonas soli* CDMK, *Paenibacillus* sp. CDME, and *Paenibacillus* sp. CDMG have not been previously reported to be capable of Mn(II) oxidation and are thus putative MnOB identified in this study. A phylogenetic tree (Fig. S3) including genera with percent sequence reads >1% as well as previously-known species with functional capabilities of interest (FeOB, MnOB, AOB, and NOB), indicates the putative MnOB identified in this study are clustered within the phyla *Actinobacteria, Firmicutes,* and *Proteobacteria* (including *Alpha-, Beta-, and Gamma-Proteobacteria*).

3.6. XANES analyses

The XANES spectra of the Mn(0), Mn(II), Mn(III), Mn(IV), and Mn (VII) standards covered K-edge energies from 6539 eV for Mn(0) to ~6557 eV for Mn(VII) (Fig. 5). The Mn K-edge XANES spectra of the Fe-filter samples (Fe-BW, Fe-An, and Fe-Sa) identified Mn phases primarily in the +3 oxidation state (Figs. 5 and 6). However, the Mn-filter inner samples (Mn-BW, Mn-An, and Mn-Sa) displayed distinctly higher Mn oxidation states of nearly +4 (Figs. 5 and 6).

The PCA and LCF analysis of the XANES data for the samples from within the Mn-filter samples revealed that birnessite (with Mn oxidation states of +3.5 to +3.9) is the dominant Mn-oxide in the Mn-BW (93.1%), Mn-An (92.5%), and Mn-Sa (100%) samples (Figs. S4 and S5).

3.7. SEM-EDS analyses

Typical biosignatures of FeOB (twisted stalks and filamentous sheaths) (Emerson et al., 2010) were observed in SEM images of the surfaces of the Fe-An samples (Fig. 7A and B). The correponding EDS analysis had a high intensity Fe peak, consistent with the presence of iron minerals (Figs. 7A and S6A). The surface coatings of the Mn-An samples generally had a coral-like morphology consistent with autocatalytic Mn-oxide formation (Bruins et al., 2015a; Cheng et al., 2018) (Fig. 7D). However, an irregular amorphous surface morphology, which has been observed in association with biogenic Mn-oxide formation (Miller et al., 2012), was also frequently observed in the Mn-An samples (Fig. 7C). The corresponding EDS analysis for the Mn-An sample showed high peak intensities for Mn and Fe (Figs. 7C and S6B).

3.8. EPR analysis

The chemically-synthesized birnessite mineral produced a signal centered at a g-factor of 2.0 and a ΔH of 2710 gauss in the EPR spectra, consistent with an abiotic origin (Kim et al., 2011) (Fig. S7A). On the other hand, the EPR spectra of Mn-BW (centrifuged solids) and Mn-Sa centered at a g-factor of around 2.0 and had ΔH values of 504 and 487 gauss, respectively (Figs. S7B and D). The ΔH values observed in the Mn-BW and Mn-Sa spectra were <600 gauss, indicating these Mn-oxides are biogenic in origin, similarly to analyses by Kim et al. (2011). The EPR spectra of Mn-BW (Fig. S7B) and Mn-Sa (Fig. S7D) samples showed a sextet of hyperfine Mn lines. These spectral patterns around g-factor = 2 are typical for Mn (III/IV) oxides that contain Mn (II) (Bruins et al., 2015b; Saisaha et al., 2013). In addition, a sharp signal at g-factor = 2.0 with a narrow ΔH of 6 gauss appeared in the EPR spectrum of the Mn-Sa sample (Fig. S7C and D), which suggests the presence of biologically-oriented organic radicals (protein) interacted with Mn (IV) (Chang et al., 2004; Nick et al., 1991).

4. Discussion

4.1. Functional microbial enrichment in the Fe and Mn filters

In this study of a pilot-scale biofiltration system, the seed populations for the microbial communities came from several sources: the natural groundwater community, the biofilter media materials, and BWS transferred from previous biofilter enrichments in the same system. Based on the differences in the microbial community diversity metrics, along with the similarity-dissimilarity analysis between the communities, there is less diversity in both biofilter communities compared to the microbial community of the influent groundwater. The biofilter communities were significantly different from the groundwater community and the Fe and Mn biofilter communities were also statistically significantly different from each other (Fig. 2 and Table S1). Over the course of biofiltration, these Fe and Mn filters accumulated abundant Fe and Mn precipitates, and the community composition of these filters showed evidence for functional enrichment tied to iron and manganese oxidation (Figs. 2, 3 and 4).

Table 2
Putative MnOB isolates from this study.

Isolate name	ENA accession no. for isolate	Mn-oxide formation (LBB I assay)	Closest match based on RDP classification (Genbank accession no.)	Identity (%)	Phylum/subphylum	Source
CDMB	LT628527	+	*Azospirillum* sp. DSM4834 (Z29623)	99%	*Alphaproteobacteria*	Mn filter
CDME	LT628529	+	*Paenibacillus* sp. MC5-1 (FJ932656)	99%	*Firmicutes*	Mn filter
CDMG	LT628531	+	*Paenibacillus* sp. MC5-1 (FJ932656)	99%	*Firmicutes*	Fe filter
CDMK	LT628533	+	*Solimonas soli* (T) DCY12 (NR_044065)	96%	*Gammaproteobacteria*	Fe filter
CDMA	LT628526	+	*Pseudomonas* sp. LAB-21 (AB051698)	99%	*Gammaproteobacteria*	Fe filter
CDMC	LT628528	+	*Mycobacterium frederiksbergense* (T) DSM 44346 (NR_025393)	99%	*Actinobacteria*	Fe filter
CDMH	LT628532	+	*Mycobacterium* sp. 22-29 (EU167977)	99%	*Actinobacteria*	Mn filter
CDML	LT628534	+	*Pseudomonas* sp. 12A 19 (AY689078)	99%	*Gammaproteobacteria*	Mn filter
CDMM	LT628535	+ (17 °C)	*Hydrogenophaga* sp. Esa.33 (AY569978)	99%	*Betaproteobacteria*	Mn filter
CDMN	LT628536	+ (8 °C)	*Hydrogenophaga* sp. Esa.33 (AY569978)	99%	*Betaproteobacteria*	Mn filter
CDMF	LT628530	−	*Rhodococcus* sp. I7 (AY177354)	99%	*Actinobacteria*	Mn filter backwash

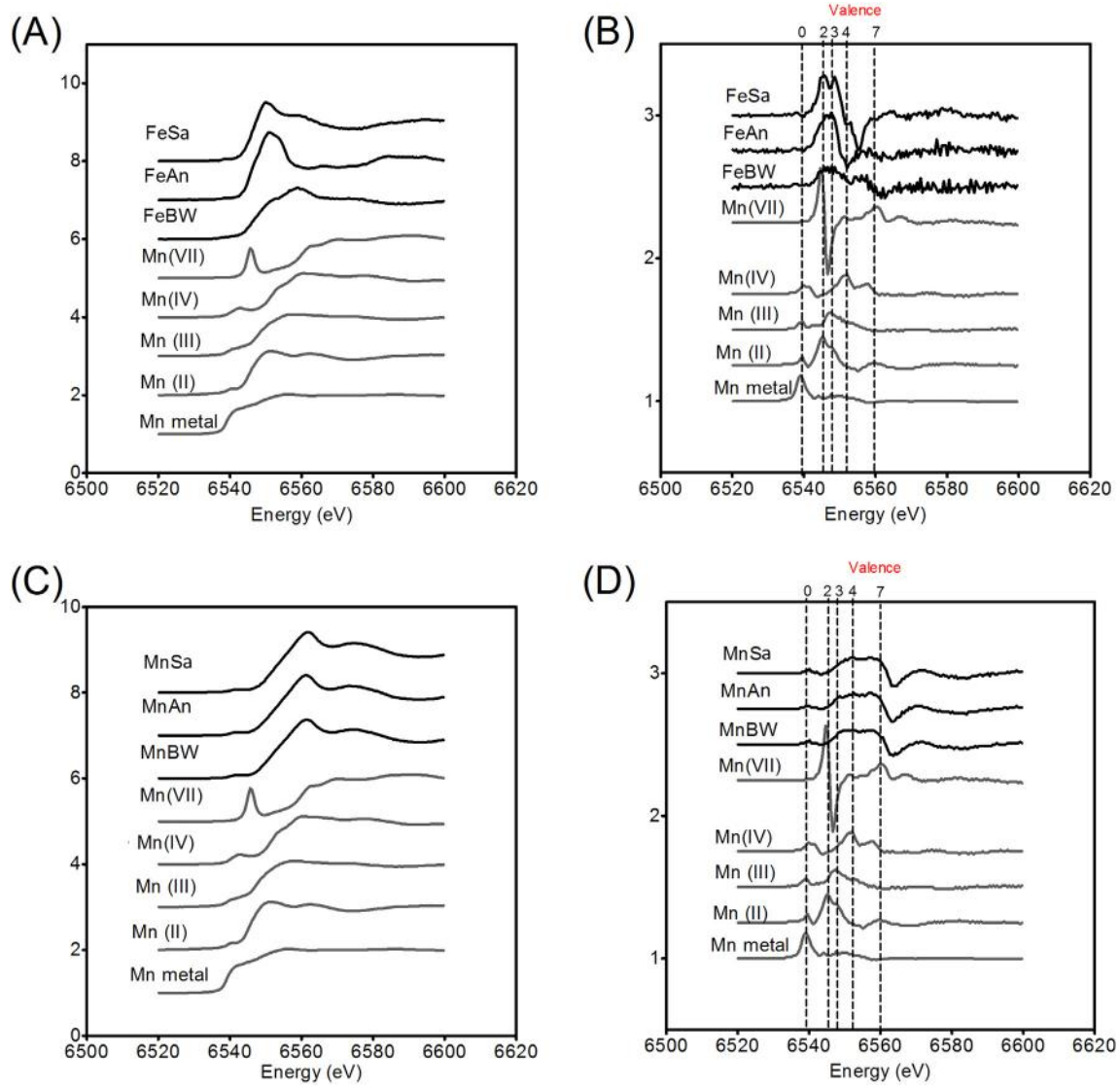

Fig. 5. The Mn K-edge XANES spectra for Fe-filter (FeBW, FeAn, and FeSa) and Mn-filter (MnBW, MnAn, and MnSa) samples: (A) the XANES spectra plotted for standards and Fe-filter samples, (B) the first derivatives of XANES spectra plotted for standards and Fe-filter samples, (C) the XANES spectra plotted for standards and Mn-filter samples, and (D) the first derivatives of XANES spectra plotted for standards and Mn-filter samples. The vertical lines indicate the absorption edge energies of Mn (0), Mn (II), Mn (III), Mn (IV), and Mn(VII) species.

Based on the heat map of representative genera (Fig. 4), community membership differences established in the biofilters during the pilot study, with clear differences in the pattern of major genera abundance between the influent natural groundwater, Fe-filter community, and Mn-filter community. The conclusion that the biofilters were enriched in microorganisms that enhance Fe(II) oxidation, Mn(II) oxidation, and nitrification is supported by the evidence presented in the microbial community heat map as well as key chemistry data throughout the biofiltration system, and the XRF analyses. Enrichment for these metabolic functions occurred during continuous operation of the biofiltration unit as it received cold groundwater during operation in the field (4 to 8 °C). This confirms that it is possible to biologically-enhance Fe and Mn removal from groundwater even at low groundwater temperatures.

The populations in the pilot biofiltration unit filters were considerably different at the genus level. Distinctive microbial enrichment patterns occurred in the in situ biofilters: (1) the Fe filter was enriched with relatives of known FeOB, and (2) the Mn filter was enriched in *Alphaproteobacteria*. The populations in the Mn filter have not (to our knowledge) been previously recognized as MnOB. The Fe filter was predominantly enriched in members of the *Betaproteobacteria* (Figs. 3 and 4) with high sequence read proportions (50 ± 10%) of known FeOB relatives in the genera *Gallionella, Sideroxydans, Ferriphaselus,* and *Hydrogenophaga*. Interestingly, the proportion of reads classified to these FeOB in the Mn filter was higher (*ca* 20–40%) than in similar studies of groundwater Mn-biofiltration system microbiology (Cheng et al., 2017; Zhang et al., 2018). Note that we did not identify *Crenothrix* in our system, but it was present in high abundance (*ca* 30%) in the study by Cheng et al. (2017). This is likely due to differences in the local groundwater microbiology, physicochemistry, and type of filter media in the pilot biofiltration system design (Breda et al., 2017); in Cheng et al. (2017) they used anthracite and Mn-coated sand, and in the present study we used anthracite and sand (without pre-existing Mn coatings). Previously known genera that include MnOB (*Pseudomonas, Hyphomicrobium, Albidiferax, Athrobacter, Acinetobacter, Zoogloea, Ralstonia*, and *Pedomicrobium*) identified in the Mn filter comprised <1% of the combined total sequence reads, and members of the *Leptothrix* genus, which are widely studied as representative MnOB (Burger et al., 2008) were not identified in the Mn filter. The only genus containing previously identified MnOB found in the Mn filter was *Planctomyces* (2 ± 2% of sequence reads, Fig. 4).

In comparison with the Fe filter (including Fe-Ef), the Mn filter contained a far greater abundance of *Alphaproteobacteria* (40 ± 10%),

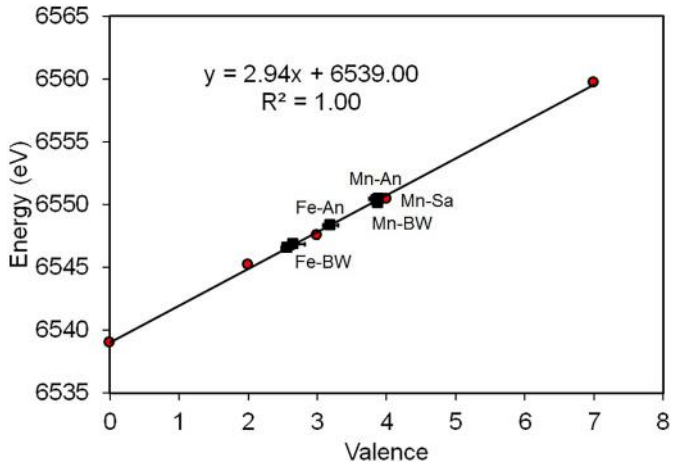

Fig. 6. The oxidation states of Mn in the Fe-filter (Fe-BW, Fe-An, and Fe-Sa) and Mn-filter (Mn-BW, Mn-An, and Mn-Sa) samples (in black) based on linear regression analysis for the Mn oxidation states and corresponding absorption edges (eV) of the XANES spectra of standards (in red): Mn (0) metal, Mn(II)SO_4, Mn(III) oxide, Mn(IV) oxide, and KMn (VII)O_4. (For interpretation of the references to color in this figure legend, the reader is referred to the web version of this article.)

which included the genera *Hirschia, Sphingopyxis, Gemmobacter, Pseudolabrys*, and 6 other unclassified genera. These genera are not known to contain Mn oxidizing species. In addition, the genera *Haliscomenobacter, Sediminibacterium, Terrimonas, Opitutus, Bdellovibrio, Thiobacillus, Hirschia, Woodsholea,* and *Sphingopyxis*, which are not known to contain MnOB, were also abundant in the Mn filter. Whether these populations were oxidizing Mn directly or were somehow indirectly involved in Mn oxidation (e.g., through co-metabolism) is not known. It is also possible they were enriched on other substrates available in the biofilter or influent groundwater (e.g., sulfur released by the anthracite).

The MnOB isolated from the Fe- and Mn-filter samples (confirmed by the formation of Mn(III/IV) precipitates) have not been previously reported as MnOB and thus represent newly identified putative MnOB (*Azospirillum* sp. CDMB, *Solimonas soli* CDMK, *Paenibacillus* sp. CDME, and *Paenibacillus* sp. CDMG). Strains CDMC, and strains CDMM and CDMN are close relatives of *Mycobacterium* sp. and *Hydrogenophaga* sp., respectively; those two organisms have only recently been reported as MnOB (Marcus et al., 2017).

4.2. Fe and Mn oxidation

Betaproteobacteria, including common FeOB, appeared in both the Fe and Mn filters. The known FeOB genera *Gallionella, Sideroxydans,* and *Hydrogenophaga* were also abundant in the Mn filter (collectively 8 ± 3% of sequence reads). Members of the *Betaproteobacteria* including *Gallionella, Sideroxydans,* and *Hydrogenophaga*, were also abundant in the effluent stream (Fe-Ef) of the Fe filter (Fig. 4). The Fe filter effluent is the influent to the Mn filter and therefore a source of FeOB populations for the Mn filter. This transfer likely contributed to the

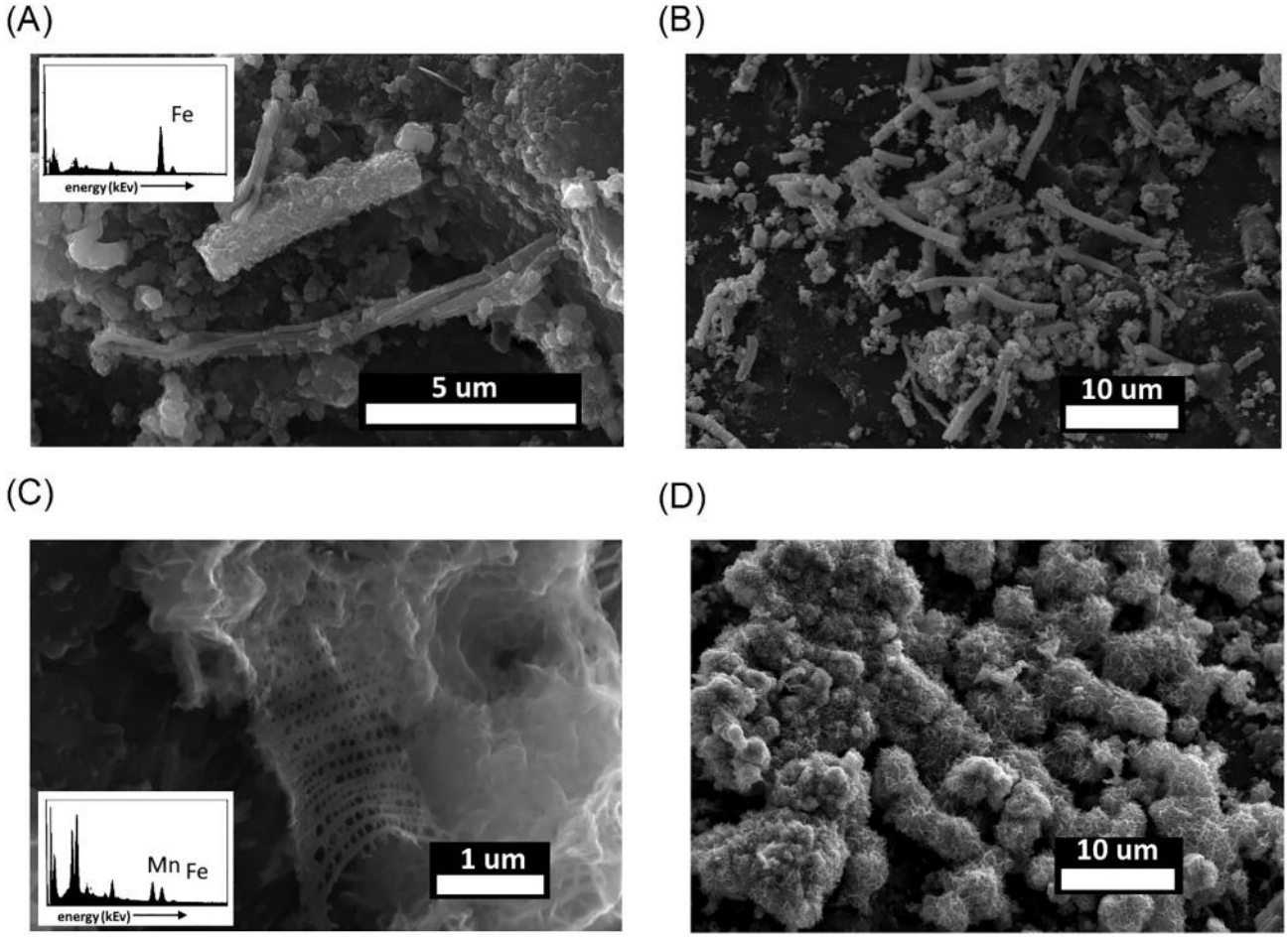

Fig. 7. Scanning electron microscopy (SEM) images of representative surface morphologies of the anthracite filter media collected on Day 183 (the end of the field experiment). Note presence of typical FeOB biosignatures in the SEM images of the surfaces of the Fe-An samples: twisted stalks (A) and filamentous sheaths (B). An amorphous, irregularly reticulated, fluffy and filamentous surface morphology (C) was observed in the SEM images of the Mn-An sample, along with a repetitious, coral-like, crystallized surface morphology (D) on other surfaces in the same Mn-An sample. Inset EDS spectra in (A) and (C) show presence of Fe and Fe/Mn in Fe filter and Mn filter, respectively (detailed version of EDS spectra presented in Fig. S6).

considerable number of OTUs shared between the Fe- and Mn-filter communities (Fig. S2).

The enrichment of FeOB in the Mn filter communities is consistent with observed changes in effluent water Fe concentration. The Fe concentration dropped by an order of magnitude after flowing through the Mn filter (i.e., from 0.018 mg/L in Mn filter influent (Fe-Ef) to 0.001 mg/L in Mn filter effluent). In addition, the Mn filter backwash sludge (Mn-BW) contained biogenic Fe oxide precipitates confirmed by XRF and SEM-EDS analysis (Dangeti et al., 2017). The FeOB in the Mn-filter likely caused the Fe(II) oxidation in the Mn filter leading to the Fe concentration decrease in the effluent and accumulation of Fe (III) oxides in the Mn biofilter. The known MnOB observed in the Mn filter (while present at low abundance) were likely partly responsible for Mn(II) oxidation observed in the Mn filter. Our study is thus consistent with Mn and Fe removal catalysed by microbial communities in the Mn filter. This is also consistent with previous single-columned biofiltration studies where Fe and Mn removal can be successfully achieved in a single column (Li et al., 2013; Yang et al., 2014). Co-existence of FeOB and MnOB is common in natural environments (e.g., ferromanganese deposits) (Northup et al., 2003; Sujith et al., 2017) and engineered environments (Fe and Mn biofilters) (Cai et al., 2015; Thapa Chhetri et al., 2013; Yang et al., 2014). It is also possible there were microbes present in the biofiltration system that were capable of both iron and manganese oxidation. For example, *Hydrogenophaga* sp. have been reported to oxidize both Fe(II) and Mn(II) (Chan, 2015; Marcus et al., 2017). This genus was present in the Mn filter (2.7 ± 0.3% of sequence reads), and it is possible this organism may have played a role in Mn and/or Fe oxidation in the Mn filter (Chan, 2015; Marcus et al., 2017). The adaptation of *Hydrogenophaga* sp. strain CDMN to the low temperatures and redox conditions present in the Mn filter (7 to 14.5 °C, >300 mV) could make this strain functionally important for biofiltration in cold climates. To the best of our knowledge, this is the first example of a *Hydrogenophaga* isolate capable of growth under psychrophilic conditions.

4.3. Biogenic birnessite as a signature of microbially-mediated Mn(II) oxidation

Based on the synchrotron-based XANES analysis, the precipitates on the Mn-filter materials exhibited Mn oxidation states between +3.7 and +4.0 (Fig. 6). Semi-quantitative LCF analysis of the XANES spectra from the Mn filter identified birnessite as the primary Mn-oxide in the Mn filter samples (>90% in all three materials, Fig. S5). In addition, the EPR analyses for these precipitates confirmed the biogenic origin (vs. abiotic origin) of the birnessite-dominated precipitates in the Mn filter samples (Mn-BW and Mn-Sa, Fig. S7). The microbial community data for the Mn filter in combination with the evidence for biogenic birnessite formation supports our findings that the Mn-filter community (most members of which have not been previously recognized as MnOB) promoted biological Mn(II) oxidation in the Mn-biofilters. This is consistent with our previous work where we observed an increase in ATP activity in the effluent from an effective Mn filter system, and ORP-pH conditions fell within the stability field for biological Mn(II) oxidation and were thus inconsistent with chemical Mn(II) oxidation (Burger et al., 2008; Dangeti et al., 2017; Mouchet, 1992).

Results from a similar study by Bruins et al. (2015a) with a pilot-scale RSF system for Mn removal from groundwater shed additional light on our results. They observed differences in EPR data that demonstrated the origins of birnessite changed from biogenic to abiotic as the biofilter aged. These authors also reported that, in the full-scale RSF systems they studied, birnessite formed by abiotic Mn(II) oxidation on the surfaces of ripened filter media. These findings suggest physicochemical Mn(II) oxidation is the dominant Mn(II) oxidation mechanism in RSF systems. RSF treatment technologies generally use higher flow velocities (e.g., 4–21 m/h) than biofiltration systems (e.g., 2–10 m/h), and often requires chemical oxidizing agents and/or pre-treatment to perform effectively (Page et al., 2006). MnOB may have initiated and/or enhanced Mn(II) oxidation in these systems, resulting in the formation of Mn(III/IV) oxides that acted as adsorbents and autocatalysts for further physicochemical Mn(II) oxidation on the Mn-oxide surface coatings during the course of the RSF treatment (Bruins et al., 2015a; Bruins et al., 2015b). Note that the role of MnOB in field-aged filter media enriched with abiotic Mn-oxides (birnessite) is not well known (Bruins et al., 2015a). Taking these previous results into consideration, the biogenic Mn(III/IV) production in the present study system in the early stages of biofiltration could promote autocatalytic Mn(II) oxidation and potentially shorten the typically long start-up period required for Mn biofiltration at low temperatures (below 15 °C).

In previous work (Dangeti et al., 2017), we confirmed with EPR analyses that biogenic birnessite formed in Mn(II)-oxidizing enrichment cultures prepared from the pilot-scale biofiltration system. Based on the EPR analyses for the filter media (present study Fig. S7) at 183 d, the Mn(II)-oxidation mechanism in the aged filter media was still dominantly biological rather than physicochemical. The characteristics of the EPR spectra for the inner Mn-filter solids (with $\Delta H < 600$ gauss), along with the results of the XANES analyses (+3.86 to +3.88 oxidation states in the Mn-filter samples, present study Figs. 5 and 6), is consistent with biogenic Mn (III/IV) oxides, which potentially contain organic radicals associated with enzymatic reactions and biological derivatives (Chang et al., 2004; Nick et al., 1991). This further supports the notion that Mn filter solids were biologically aged in the field (i.e., that the source of the Mn oxides in the filters was biologically derived). Furthermore, an amorphous, irregularly reticulated, fluffy, and filamentous surface morphology, which is characteristic of biogenic Mn-oxides (Miller et al., 2012), was present in the SEM images for the Mn filter media (Mn-An; Fig. 7C). In summary, biological Mn(II) oxidation, indicated by the characteristic EPR signal for biogenic Mn-oxide formation, may be responsible not only for the initiation but also the maintenance of biological Mn(II) oxidation in low temperature biofiltration systems such as the one described in this study.

Evidence for autocatalytic Mn(II) oxidation on the biofiltration media surface coatings was also observed. A repetitious, coral-like, crystallized surface morphology on other surfaces in the same Mn-filter media (Mn-An) was observed in the SEM images (Fig. 7D). This surface morphology reflects the autocatalytic nature of some Mn-oxide surface coatings, as reported by Jiang et al. (2010), Bruins et al. (2015a), and Cheng et al. (2018). Such variations in the surface morphology of the aged filter media in this study imply both biogenic and abiotic Mn(II) oxidation occurred in the on-site Mn filter, rather than a complete conversion from one dominant oxidation mechanism to another (biological to physicochemical) as observed in the RSF study by Bruins et al. (2015a).

Biogenic Mn-oxides act as strong oxidizing agents with high surface areas that potentially accelerate Mn(II) oxidation (Learman et al., 2011). The formation of biogenic birnessite is therefore advantageous for initiating, enhancing, and maintaining biological Mn(II) oxidation. Birnessite is an intermediate product of the Mn oxidation pathway and pyrolusite (Mn(IV) oxide) is thermodynamically favored as the final oxidation product (Bruins et al., 2015b; Stumm and Morgan, 1996). In our study, pyrolusite is a minor mineral and birnessite is the dominant Mn-oxide in the filter media. This implies that, in low-temperature groundwater biofiltration systems, the continuous supply of biogenic birnessite by metabolically-active MnOB adapted to low on-site temperatures may play a critical role in shortening the start-up period, maintaining Mn(II) oxidative activity, and further increasing the rate of Mn(II) removal. As a result, this study suggests the formation of biogenic birnessite can be a key indicator, and even a prerequisite, for successful biofiltration systems that combine biological and autocatalytic Mn(II) oxidation at low temperatures in cold climates.

5. Conclusions

In this study of a continuous, flow-through, on-site biofiltration system for cold groundwater, high-throughput sequencing of the microbial community, coupled with mineralogical and spectral analyses of the field-aged filter media, was used to confirm enrichment of microbial communities that microbially mediate oxidation of Fe(II) and Mn(II) and remove these constituents from the water as oxide minerals. The microbial community composition and function differed between the influent groundwater, Fe filter, and the Mn filter. The microbial communities in the Fe and Mn filters included populations associated with Fe(II) and Mn(II) oxidation; however, significant numbers of new putative MnOB appeared in both biofilters, including several organisms isolated in this study using MnOB enrichment media (isolates *Azospirillum* sp. CDMB, *Solimonas soli* CDMK, *Paenibacillus* sp. CDME, and *Paenibacillus* sp. CDMG). This study identified a new strain of *Hydrogenophaga* sp. that can oxidize manganese and generate Mn(III/IV) oxides even at low temperatures (8 to 15 °C).

Biogenic birnessite, a mineral that could promote further autocatalysis of Mn(II) oxidation, dominated the Mn oxides in the pilot biofiltration system, even as the system matured. Biogenic birnessite can be a robust indicator for the occurrence of biological Mn(II) oxidation and is potentially a driver for subsequent autocatalytic oxidation of Mn(II), based on the data presented in both the present work and previous studies (Bruins et al., 2015a; Dangeti et al., 2017). Effective biofiltration of Mn from groundwater in cold climates is likely accelerated when biogenic birnessite is present.

The findings in this study provide evidence that contributes to efforts to improve affordable and effective water treatment options for regions where cold groundwater conditions are common. It is also highly relevant for water treatment in remote areas where treatment technologies can be difficult to monitor and manage, and social license to operate issues (local community and other stakeholder concerns) often accompany use of chemical treatments (e.g., remote northern regions of Canada). As demonstrated in this study, biofiltration is a viable approach to remove iron, manganese, and ammonia in these cold groundwater systems, and mineralogical and microbiological approaches can be used to monitor biofiltration system efficacy and function.

Credit author statement

BaR and BrR designed and operated the pilot-scale biofiltration unit at Langham Water Treatment Plant; SRD; JMM, and WC designed the downstream laboratory experiments and analyses using the groundwater collected in the field; SD conducted the lab experiments; SRD and JMM collected XANES data, and analysis was performed by SRD; Jonathan Vyskocil (JV) prepared and executed the sequencing data pipeline in mothur; SRD conducted data analysis and interpretation, and manuscript preparation, under the supervision of WC, JMM, and BaR. All authors read and approved the final manuscript.

Declaration of competing interest

The authors declare the following financial interests/personal relationships which may be considered as potential competing interests: Note that three of the authors (Babak Roshani, Bryan Rindall, and Sandeepraja Dangeti) on this manuscript are employees of one of our project funders (Delco Water Division of Delco Automation Inc.). We have indicated this in the competing interests statement in the manuscript according to the author guideline. We welcome your suggestions on additional wording for the competing interests statement if you believe they are necessary.

Acknowledgements

We thank L. Sawatzky, operator at Langham Water Treatment, for support in pilot-scale biofilter operation. XANES analyses were performed at the Canadian Light Source, which is supported by the National Research Council of Canada (NSERC), the Canadian Institutes of Health Research, the Province of Saskatchewan, Western Economic Diversification Canada, and the University of Saskatchewan. We thank J. Dynes for provision of Mn-oxide standards; D. Muir for assistance with beamtime at the CLS; J. Stobbs for assistance with lab activities at CLS; S. Samaila, J. Essilfie-Dughan, and V. Bondici for assistance with XANES data interpretation; R. Sammynaiken for assistance with EPR analyses at the Saskatchewan Structural Sciences Centre; H. Yin for assistance in the Environmental Engineering Laboratory, University of Saskatchewan; and five anonymous reviewers for their constructive criticism.

Funding

This research was supported by the NSERC grants [grant numbers CRDPJ 487008-15, EGP 468673-14, and RGPIN-2014-459 05902] to Wonjae Chang [WJC] and grant [grant number RGPIN-2014-03719] to Joyce M. McBeth [JMM]; a MITACs Accelerate grant [grant number IT06847] and Canada Foundation for Innovation (CFI) John R. Evans Leaders Fund (JELF) grant [grant number 33982] to WJC. The work presented in this study was also funded by the Delco Water Division of Delco Automation Inc.

Author contributions

BaR and BrR designed and operated the pilot-scale biofiltration unit at Langham Water Treatment Plant; SRD; JMM, and WC designed the downstream laboratory experiments and analyses using the groundwater collected in the field; SRD conducted the lab experiments; SRD and JMM collected XANES data, and analysis was performed by SRD; Jonathan Vyskocil (JV) prepared and executed the sequencing data pipeline in mothur; SRD conducted data analysis and interpretation, and manuscript preparation, under the supervision of WC, JMM, and BaR. All authors read and approved the final manuscript.

Appendix A. Supplementary data

Supplementary data to this article can be found online at https://doi.org/10.1016/j.scitotenv.2019.136386.

References

Akob, D.M., Bohu, T., Beyer, A., Schäffner, F., Händel, M., Johnson, C.A., et al., 2014. Identification of Mn(II)-oxidizing bacteria from a low-pH contaminated former uranium mine. Appl. Environ. Microbiol. 80, 5086–5097. https://doi.org/10.1128/AEM.01296-14.

Arp, D.J., Sayavedra-Soto, L.A., Hommes, N.G., 2002. Molecular biology and biochemistry of ammonia oxidation by *Nitrosomonas europaea*. Arch. Microbiol. 178, 250–255. https://doi.org/10.1007/s00203-002-0452-0.

Berbenni, P., Pollice, A., Canziani, R., Stabile, L., Nobili, F., 2000. Removal of iron and manganese from hydrocarbon-contaminated groundwaters. Bioresour. Technol. 74, 109–114. https://doi.org/10.1016/S0960-8524(00)00003-1.

Beukes, L.S., Schmidt, S., 2012. Isolation and characterization of a manganese-oxidizing bacterium from a biofiltration system for the treatment of borehole water in KwaZulu-Natal (South Africa). Engineering in Life Sciences 12, 544–552. https://doi.org/10.1002/elsc.201100153.

Blackwood, C.B., Hudleston, D., Zak, D.R., Buyer, J.S., 2007. Interpreting ecological diversity indices applied to terminal restriction fragment length polymorphism data: insights from simulated microbial communities. Appl. Environ. Microbiol. 73, 5276–5283. https://doi.org/10.1128/aem.00514-07.

Bouchard, M.F., Sauvé, S., Barbeau, B., Legrand, M., Brodeur, M.-È., Bouffard, T., et al., 2011. Intellectual impairment in school-age children exposed to manganese from drinking water. Environ. Health Perspect. 119, 138–143. https://doi.org/10.1289/ehp.1002321.

Breda, I.L., Ramsay, L., Roslev, P., 2017. Manganese oxidation and bacterial diversity on different filter media coatings during the start-up of drinking water biofilters. J. Water Supply Res. Technol. AQUA 66, 641–650. https://doi.org/10.2166/aqua.2017.084.

Bruins, J.H., Petrusevski, B., Slokar, Y.M., Huysman, K., Joris, K., Kruithof, J.C., et al., 2015a. Biological and physico-chemical formation of Birnessite during the ripening of

manganese removal filters. Water Res. 69, 154–161. https://doi.org/10.1016/j.watres.2014.11.019.
Bruins, J.H., Petrusevski, B., Slokar, Y.M., Kruithof, J.C., Kennedy, M.D., 2015b. Manganese removal from groundwater: characterization of filter media coating. Desalin. Water Treat. 55, 1851–1863. https://doi.org/10.1080/19443994.2014.927802.
Burger, M.S., Krentz, C.A., Mercer, S.S., Gagnon, G.A., 2008. Manganese removal and occurrence of manganese oxidizing bacteria in full-scale biofilters. J. Water Supply Res. Technol. AQUA 57, 351–359. https://doi.org/10.2166/aqua.2008.050.
Cai, Y., Li, D., Liang, Y., Luo, Y., Zeng, H., Zhang, J., 2015. Effective start-up biofiltration method for Fe, Mn, and ammonia removal and bacterial community analysis. Bioresour. Technol. 176, 149–155. https://doi.org/10.1016/j.biortech.2014.11.025.
Caporaso, J.G., Lauber, C.L., Walters, W.A., Berg-Lyons, D., Lozupone, C.A., Turnbaugh, P.J., et al., 2011. Global patterns of 16S rRNA diversity at a depth of millions of sequences per sample. Proc. Natl. Acad. Sci. 108, 4516–4522. https://doi.org/10.1073/pnas.1000080107.
Cerrato, J.M., Falkinham Iii, J.O., Dietrich, A.M., Knocke, W.R., McKinney, C.W., Pruden, A., 2010. Manganese-oxidizing and -reducing microorganisms isolated from biofilms in chlorinated drinking water systems. Water Res. 44, 3935–3945. https://doi.org/10.1016/j.watres.2010.04.037.
Chan, C.S.-Y., 2015. The Effects of Fe-oxidizing Microorganisms on Post-biostimulation Permeability Reduction and Oxidative Processes at the Rifle IFRC Site. DOE-UDEL-07116-1. USDOE Office of Science (SC), Biological and Environmental Research (BER), p. 12. https://doi.org/10.2172/1188716.
Chang, C.H., Svedružić, D., Ozarowski, A., Walker, L., Yeagle, G., Britt, R.D., et al., 2004. EPR spectroscopic characterization of the manganese center and a free radical in the oxalate decarboxylase reaction: identification of a tyrosyl radical during turnover. J. Biol. Chem. 279, 52840–52849. https://doi.org/10.1074/jbc.M402345200.
Cheng, Q., Nengzi, L., Bao, L., Huang, Y., Liu, S., Cheng, X., et al., 2017. Distribution and genetic diversity of microbial populations in the pilot-scale biofilter for simultaneous removal of ammonia, iron and manganese from real groundwater. Chemosphere 182, 450–457. https://doi.org/10.1016/j.chemosphere.2017.05.075.
Cheng, Y., Huang, T., Cheng, L., Sun, Y., Zhu, L., Li, Y., 2018. Structural characteristic and ammonium and manganese catalytic activity of two types of filter media in groundwater treatment. J. Environ. Sci. (China) 72, 89–97. https://doi.org/10.1016/j.jes.2017.12.014.
Cheng, Q., Huang, Y., Nengzi, L., Liu, J., Zhang, J., 2019. Performance and microbial community profiles in pilot-scale biofilter for ammonia, iron and manganese removal at different dissolved oxygen concentrations. World J. Microbiol. Biotechnol. 35 (43). https://doi.org/10.1007/s11274-019-2617-x.
Chin, K.J., Liesack, W., Janssen, P.H., 2001. *Opitutus terrae* gen. nov., sp. nov., to accommodate novel strains of the division *Verrucomicrobia*; isolated from rice paddy soil. Int. J. Syst. Evol. Microbiol. 51, 1965–1968. https://doi.org/10.1099/00207713-51-6-1965.
Cole, J.R., Wang, Q., Fish, J.A., Chai, B., McGarrell, D.M., Sun, Y., et al., 2014. Ribosomal Database Project: data and tools for high throughput rRNA analysis. Nucleic Acids Res. 42, D633–D642. https://doi.org/10.1093/nar/gkt1244.
Dangeti, S., Roshani, B., Rindall, B., McBeth, J.M., Chang, W., 2017. Biofiltration field study for cold Fe(II)- and Mn(II)-rich groundwater: accelerated Mn(II) removal kinetics and cold-adapted Mn(II)-oxidizing microbial populations. Water Quality Research Journal 52, 229–242. https://doi.org/10.2166/wqrj.2017.006.
Edgar, R.C., Haas, B.J., Clemente, J.C., Quince, C., Knight, R., 2011. UCHIME improves sensitivity and speed of chimera detection. Bioinformatics 27, 2194–2200. https://doi.org/10.1093/bioinformatics/btr381.
Emerson, D., Fleming, E.J., McBeth, J.M., 2010. Iron-oxidizing bacteria: an environmental and genomic perspective. Annu. Rev. Microbiol. 64, 561–583. https://doi.org/10.1146/annurev.micro.112408.134208.
Hallbeck, L., Ståhl, F., Pedersen, K., 1993. Phylogeny and phenotypic characterization of the stalk-forming and iron-oxidizing bacterium *Gallionella ferruginea*. Microbiology 139, 1531–1535. https://doi.org/10.1099/00221287-139-7-1531.
Hardie, A., Dynes, J., Kozak, L., Huang, P., 2007. Influence of polyphenols on the integrated polyphenol-maillard reaction humification pathway as catalyzed by birnessite. Annals of Environmental Science 1, 91–110.
Health Canada, 2019. Guidelines for Canadian drinking water quality summary table. Water and Air Quality Bureau Healthy Environments and Consumer Safety Branch, (Ed.). Health Canada, Ottawa, Ontario, p. 26.
Jiang, S., Kim, D.G., Kim, J., Ko, S.O., 2010. Characterization of the biogenic manganese oxides produced by *Pseudomonas putida* strain MnB1. Environmental Engineering Research (4), 183–190 https://doi.org/10.4491/eer.2010.15.4.183.
Kato, S., Krepski, S., Chan, C., Itoh, T., Ohkuma, M., 2014. Ferriphaselus amnicola gen. nov., sp. nov., a neutrophilic, stalk-forming, iron-oxidizing bacterium isolated from an iron-rich groundwater seep. Int. J. Syst. Evol. Microbiol. 64, 921–925. https://doi.org/10.1099/ijs.0.058487-0.
Katsoyiannis, I.A., Zouboulis, A.I., 2004. Biological treatment of Mn(II) and Fe(II) containing groundwater: kinetic considerations and product characterization. Water Res. 38, 1922–1932. https://doi.org/10.1016/j.watres.2004.01.014.
Kim, S.S., Bargar, J.R., Nealson, K.H., Flood, B.E., Kirschvink, J.L., Raub, T.D., et al., 2011. Searching for biosignatures using electron paramagnetic resonance (EPR) analysis of manganese oxides. Astrobiology 11, 775–786. https://doi.org/10.1089/ast.2011.0619.
Kuypers, M.M.M., Marchant, H.K., Kartal, B., 2018. The microbial nitrogen-cycling network. Nat. Rev. Microbiol. 16, 263. https://doi.org/10.1038/nrmicro.2018.9.
Learman, D.R., Wankel, S.D., Webb, S.M., Martinez, N., Madden, A.S., Hansel, C.M., 2011. Coupled biotic–abiotic Mn(II) oxidation pathway mediates the formation and structural evolution of biogenic Mn oxides. Geochim. Cosmochim. Acta 75, 6048–6063. https://doi.org/10.1016/j.gca.2011.07.026.
Li, X., Chu, Z., Liu, Y., Zhu, M., Yang, L., Zhang, J., 2013. Molecular characterization of microbial populations in full-scale biofilters treating iron, manganese and ammonia containing groundwater in Harbin, China. Bioresour. Technol. 147, 234–239. https://doi.org/10.1016/j.biortech.2013.08.008.
Liu, J., Wang, Z., Belchik, S.M., Edwards, M.J., Liu, C., Kennedy, D.W., et al., 2012. Identification and characterization of MtoA: a decaheme *c*-type cytochrome of the neutrophilic Fe (II)-oxidizing bacterium *Sideroxydans lithotrophicus* ES-1. Front. Microbiol. 3, 37. https://doi.org/10.3389/fmicb.2012.00037.
Lücker, S., Wagner, M., Maixner, F., Pelletier, E., Koch, H., Vacherie, B., et al., 2010. A Nitrospira metagenome illuminates the physiology and evolution of globally important nitrite-oxidizing bacteria. Proc. Natl. Acad. Sci. 107, 13479–13484. https://doi.org/10.1073/pnas.1003860107.
Marcus, D.N., Pinto, A., Anantharaman, K., Ruberg, S.A., Kramer, E.L., Raskin, L., et al., 2017. Diverse manganese (II)-oxidizing bacteria are prevalent in drinking water systems. Environ. Microbiol. Rep. 9, 120–128. https://doi.org/10.1111/1758-2229.12508.
Miller, A.Z., Dionísio, A., Braga, M.A.S., Hernández-Mariné, M., Afonso, M.J., Muralha, V.S.F., et al., 2012. Biogenic Mn oxide minerals coating in a subsurface granite environment. Chem. Geol. 322, 181–191. https://doi.org/10.1016/j.chemgeo.2012.07.005.
Mouchet, P., 1992. From conventional to biological removal of Fe and Mn in France. J. Am. Water Works Assoc. 84, 158–166. https://doi.org/10.1002/j.1551-8833.1992.tb07342.x.
Nam, K.-W., Kim, M.G., Kim, K.-B., 2007. In situ Mn K-edge X-ray absorption spectroscopy studies of electrodeposited manganese oxide films for electrochemical capacitors. J. Phys. Chem. C 111, 749–758. https://doi.org/10.1021/jp063130o.
Nealson, K.H., 2006. The manganese-oxidizing bacteria. The Prokaryotes 5, 222–231.
Nick, R.J., Ray, G.B., Fish, K.M., Spiro, T.G., Groves, J.T., 1991. Evidence for a weak Mn: O bond and a non-porphyrin radical in manganese-substituted horseradish peroxidase compound I. J. Am. Chem. Soc. 113, 1838–1840.
Northup, D.E., Barns, S.M., Yu, L.E., Spilde, M.N., Schelble, R.T., Dano, K.E., et al., 2003. Diverse microbial communities inhabiting ferromanganese deposits in Lechuguilla and Spider Caves. Environ. Microbiol. 5, 1071–1086. https://doi.org/10.1046/j.1462-2920.2003.00500.x.
Page D., Wakelin S., van Leeuwen J., Dillon P. 2006. Review of biofiltration processes relevant to water reclamation via aquifers. CSIRO Land and Water Science Report, 47/06, CSIRO, Canberra, Australia. pp. 72.
Post, J.E., 1999. Manganese oxide minerals: crystal structures and economic and environmental significance. Proc. Natl. Acad. Sci. 96, 3447–3454. https://doi.org/10.1073/pnas.96.7.3447.
Ravel, B., Newville, M., 2005. ATHENA, ARTEMIS, HEPHAESTUS: data analysis for X-ray absorption spectroscopy using IFEFFIT. J. Synchrotron Radiat. 12, 537–541. https://doi.org/10.1107/S0909049505012719.
Sahabi, D.M., Takeda, M., Suzuki, I., Koizumi, J., 2009. Removal of Mn^{2+} from water by "aged" biofilter media: the role of catalytic oxides layers. J. Biosci. Bioeng. 107, 151–157. https://doi.org/10.1016/j.jbiosc.2008.10.013.
Saisaha, P., de Boer, J.W., Browne, W.R., 2013. Mechanisms in manganese catalysed oxidation of alkenes with H_2O_2. Chem. Soc. Rev. 42, 2059–2074. https://doi.org/10.1039/C2CS35443H.
Schloss, P.D., Handelsman, J., 2005. Introducing DOTUR, a computer program for defining operational taxonomic units and estimating species richness. Appl. Environ. Microbiol. 71, 1501–1506. https://doi.org/10.1128/AEM.71.3.1501-1506.2005.
Schloss, P.D., Westcott, S.L., Ryabin, T., Hall, J.R., Hartmann, M., Hollister, E.B., et al., 2009. Introducing mothur: open-source, platform-independent, community-supported software for describing and comparing microbial communities. Appl. Environ. Microbiol. 75, 7537–7541. https://doi.org/10.1128/AEM.01541-09.
Schloss, P.D., Gevers, D., Westcott, S.L., 2011. Reducing the effects of PCR amplification and sequencing artifacts on 16S rRNA-based studies. PLoS One 6, e27310. https://doi.org/10.1371/journal.pone.0027310.
Schmidt, J.M., Sharp, W.P., Starr, M.P., 1981. Manganese and iron encrustations and other features of *Planctomyces crassus* Hortobágyi 1965, morphotype Ib of the *Blastocaulis-Planctomyces* group of budding and appendaged bacteria, examined by electron microscopy and X-ray micro-analysis. Curr. Microbiol. 5, 241–246. https://doi.org/10.1007/BF01571155.
Sjöberg, S., Callac, N., Allard, B., Smittenberg, R.H., Dupraz, C., 2018. Microbial communities inhabiting a rare earth element enriched birnessite-type manganese deposit in the Ytterby mine, Sweden. Geomicrobiol J. 35, 657–674. https://doi.org/10.1080/01490451.2018.1444690.
Stumm, W., Morgan, J.J., 1996. Chemical Equilibria and Rates in Natural Waters. John Wiley & Sons, Inc, New York.
Sujith, P.P., Gonsalves, M.J.B.D., Bhonsle, S., Shaikh, S., LokaBharathi, P.A., 2017. Bacterial activity in hydrogenetic ferromanganese crust from the Indian Ocean: a combined geochemical, experimental and pyrosequencing study. Environ. Earth Sci. 76 (191). https://doi.org/10.1007/s12665-017-6495-y.
Tebo, B.M., Johnson, H.A., McCarthy, J.K., Templeton, A.S., 2005. Geomicrobiology of manganese(II) oxidation. Trends Microbiol. 13, 421–428. https://doi.org/10.1016/j.tim.2005.07.009.
Tebo, B.M., Clement, B.G., Dick, G.J., 2007. Biotransformations of manganese. In: Hurst, C.J., Crawford, R.L., Garland, J.L., Lipson, D.A., Mills, A.L., Stetzenbach, L.D. (Eds.), Manual of Environmental Microbiology. ASM Press, Washington, DC, pp. 1223–1238.
Tekerlekopoulou, A.G., Pavlou, S., Vayenas, D.V., 2013. Removal of ammonium, iron and manganese from potable water in biofiltration units: a review. J. Chem. Technol. Biotechnol. 88, 751–773. https://doi.org/10.1002/jctb.4031.
Thapa Chhetri, R., Suzuki, I., Takezaki, J., Tabusa, H., Takeda, M., Koizumi, J., 2013. Bacterial diversity in biological filtration plant for the removal of iron and manganese from groundwater. Journal of Water and Environment Technology 11, 33–47. https://doi.org/10.2965/jwet.2013.33.
Wang, Q., Garrity, G.M., Tiedje, J.M., Cole, J.R., 2007. Naive Bayesian classifier for rapid assignment of rRNA sequences into the new bacterial taxonomy. Appl. Environ. Microbiol. 73, 5261–5267. https://doi.org/10.1128/AEM.00062-07.

Yang, L., Li, X., Chu, Z., Ren, Y., Zhang, J., 2014. Distribution and genetic diversity of the microorganisms in the biofilter for the simultaneous removal of arsenic, iron and manganese from simulated groundwater. Bioresour. Technol. 156, 384–388. https://doi.org/10.1016/j.biortech.2014.01.067.

Yue, J.C., Clayton, M.K., 2005. A similarity measure based on species proportions. Communications in Statistics - Theory and Methods 34, 2123–2131. https://doi.org/10.1080/STA-200066418.

Zhang, Y., Sun, R., Zhou, A., Zhang, J., Luan, Y., Jia, J., et al., 2018. Microbial community response reveals underlying mechanism of industrial-scale manganese sand biofilters used for the simultaneous removal of iron, manganese and ammonia from groundwater. AMB Express 8, 2. https://doi.org/10.1186/s13568-017-0534-7.